



HAL
open science

Extracellular vesicles: major actors of heterogeneity in tau spreading among human tauopathies

Elodie Leroux, Romain Perbet, Raphaëlle Caillerez, Kevin Richetin, Sarah Lieger, Jeanne Espourteille, Thomas Bouillet, Séverine Bégard, Clément Danis, Anne Loyens, et al.

► To cite this version:

Elodie Leroux, Romain Perbet, Raphaëlle Caillerez, Kevin Richetin, Sarah Lieger, et al.. Extracellular vesicles: major actors of heterogeneity in tau spreading among human tauopathies. *Molecular Therapy*, 2021, pp.S1525-0016(21)00475-5. 10.1016/j.ymthe.2021.09.020 . inserm-03356237

HAL Id: inserm-03356237

<https://inserm.hal.science/inserm-03356237>

Submitted on 27 Sep 2021

HAL is a multi-disciplinary open access archive for the deposit and dissemination of scientific research documents, whether they are published or not. The documents may come from teaching and research institutions in France or abroad, or from public or private research centers.

L'archive ouverte pluridisciplinaire **HAL**, est destinée au dépôt et à la diffusion de documents scientifiques de niveau recherche, publiés ou non, émanant des établissements d'enseignement et de recherche français ou étrangers, des laboratoires publics ou privés.

1 Extracellular vesicles: major actors of heterogeneity in tau spreading among human tauopathies

2
3
4 Elodie Leroux^{1†}, Romain Perbet^{1†}, Raphaëlle Caillerez¹, Kevin Richetin^{2,3,4}, Sarah Lieger¹, Jeanne Espourteille²,
5 Thomas Bouillet¹, Séverine Bégard¹, Clément Danis¹, Anne Loyens¹, Nicolas Toni², Nicole Déglon^{3,4}, Vincent
6 Deramecourt¹, Susanna Schraen-Maschke¹, Luc Buée^{1*} and Morvane Colin^{1*}

7
8 Short title: EVs in pathological tau propagation

9
10 1. Univ. Lille, Inserm, CHU-Lille, Lille Neuroscience & Cognition, F-59000 Lille, France.

11 2. Department of Psychiatry, Center for Psychiatric Neurosciences, Lausanne University Hospital (CHUV) and
12 University of Lausanne, 1011- Lausanne, Switzerland

13 3. Lausanne University Hospital (CHUV) and University of Lausanne, Neuroscience Research Center (CRN),
14 Laboratory of Cellular and Molecular Neurotherapies, 1011 – Lausanne, Switzerland

15 4. Lausanne University Hospital (CHUV) and University of Lausanne, Department of Clinical Neuroscience
16 (DNC), Laboratory of Cellular and Molecular Neurotherapies, 1011 – Lausanne, Switzerland

17
18
19
20
21
22 †. Equal contributors

23
24
25
26
27
28
29
30
31
32 * Corresponding authors:

33 Drs M. Colin & L. Buée

34 Lille Neuroscience & Cognition, Inserm UMR-S 1172, ‘Alzheimer & tauopathies’

35 Univ. Lille, Fac. de Médecine – pole recherche

36 Bâtiment Biserte, rue Polonovski

37 59045 Lille Cedex, France

38 Tel: 33-3-20 62 20 73, Fax: 33-2-20 53 85 62

39 M.C. (morvane.colin@inserm.fr, ORCID 0000-0003-0611-4167) and L.B. (luc.buee@inserm.fr, ORCID 0000-
40 0002-6261-4230)

41
42
43
44
45
46
47
48
49
50
51
52
53
54
55
56
57
58
59
60
61
62
63
64
65
66
67
68
69
70
71
72

Abstract-

Tauopathies are neurodegenerative diseases characterized by tau inclusions in brain cells. Seed-competent tau species have been suggested to spread from cell to cell in a stereotypical manner, indicating that this may involve a prion-like mechanism. Although the intercellular mechanisms of transfer are unclear, extracellular vesicles (EVs) could be potential shuttles. We assessed this in humans by preparing vesicles from fluids (Brain-derived enriched extracellular vesicles; BD-EVs). These latter were isolated from different brain regions in various tauopathies and their seeding potential was assessed *in vitro* and *in vivo*. We observed considerable heterogeneity among tauopathies and brain regions. The most striking evidence was coming mainly from Alzheimer’s disease where the BD-EVs clearly contain pathological species that can induce tau lesions *in vivo*. The results support the hypothesis that BD-EVs, participate in the prion-like propagation of tau pathology among tauopathies, and there may be implications for diagnostic and therapeutic strategies.

Key words: biological fluids, exosomes, microvesicles, prion-like propagation, tauopathies, Alzheimer’s disease

73 **Introduction**

74 Tau, a microtubule-associated protein,¹ aggregates into filaments in Alzheimer's disease (AD) and in other related
75 and heterogeneous diseases called tauopathies, which are characterized by the intracellular accumulation of
76 hyperphosphorylated tau.² An alternative splicing mechanism gives rise to six major isoforms of tau that coexist
77 in the human brain, which either have three or four repeated sequences of the microtubule-binding region (3R-tau
78 and 4R-tau).³ In AD, tau protein principally aggregates into paired helical filaments (3R-tau and 4R-tau) within
79 the neurons, while in progressive supranuclear palsy (PSP), tau aggregates consist of straight filaments (4R-tau)
80 and are found in both the neurons and the glia. In Pick's disease (PiD), specific neuronal tau inclusions are seen,
81 known as Pick bodies, in which 3R-tau aggregates form a spherical shape within the neuronal cell body. These
82 different tauopathy filaments are beginning to be better described and are different among tauopathies.⁴⁻⁷

83 In AD, the most common tauopathy, the progression of neurodegeneration in the brain correlates very well with
84 the clinical signs of the disease at each stage. It follows a sequential, hierarchical progression of brain involvement
85 in a pattern that is similar for all patients: the hippocampal formation, the polymodal association areas, the
86 unimodal association regions, and in the final stages of the disease, the entire cerebral cortex.^{8,9} This stereotypical
87 hierarchy of neurodegeneration is known in the literature as the Braak stages.⁸ Specific hierarchical pathways have
88 also been described for PSP,^{10,11} argyrophilic grain disease,¹² and PiD.¹³ These patterns of progression have been
89 considered as steps in the propagation of neurodegeneration and have led to the hypothesis of a prion-like tau
90 propagation.³ In this hypothesis, an abnormal tau protein conformation would lead to the prion-like
91 transconformation of normal tau proteins into abnormal ones. This would be followed by the secretion of
92 pathological seeds, which would then be internalized by healthy neurons thus transmitting the pathology.

93 While tau was first identified as a protein implicated in the assembly and stabilization of microtubules,¹ it is now
94 described as a pleiotropic protein with various cellular locations.¹⁴ It is known that the protein can be secreted by
95 unconventional pathways, mostly in a free form,¹⁵⁻²⁵ and it has also been found in extracellular vesicles (EVs).²⁶
96 EVs have two main cellular origins: (1) EVs known as exosomes are generated from multivesicular bodies,
97 containing intraluminal vesicles, that are secreted into the extracellular fluid, and (2) EVs known as ectosomes
98 originate from direct plasma membrane budding.²⁷ These vesicles have the capacity to transfer many biologically
99 active molecules between cells, and they are known to be dysregulated in many disorders.²⁸ While the secretion
100 of tau in EVs has been validated using many cell and animal models,²⁹ there is little data concerning the transfer
101 of pathological tau species or seeds between cells,³⁰ to induce a seeding process in humans.³¹ According to the
102 hypothesis of prion-like propagation, once inside the recipient cell, the seeds present in EVs seem to be released
103 from the endolysosome and lead to the recruitment and misfolding of normal endogenous proteins.³²

104 While tau aggregation is a common feature of tauopathies, a huge heterogeneity exists between and within these
105 pathologies. Recent data suggest, for instance, that pathological tau seeds in human brains differ between
106 tauopathies,³³ and also within a particular tauopathy, as has been shown for AD.³⁴ Additionally, the affected brain
107 pathways differ between AD and other tauopathies, and some cell populations are more vulnerable than others.^{8,}
108 ¹¹⁻¹³ It is thus essential to understand the underlying reasons for this heterogeneity before designing a specific
109 therapeutic approach.

110 In this work, we focused our attention on EVs because they have a certain selectivity in terms of the target cell
111 due to the presence of numerous ligands and receptors on their surface.²⁷ They therefore represent a unique
112 intercellular delivery vehicle for transferring pathological species from one specific neuronal population to
113 another, and they could explain the differing cell vulnerability seen in tauopathies. The work presented here aims
114 to compare the transmission of tau pathology via EVs that are present within brain-derived-fluids (BD-fluids) of
115 patients with various tauopathies. Although EVs isolated from the cerebrospinal fluid,³⁵⁻³⁷ and plasma,³⁸⁻⁴³ contain
116 tau, the interstitial fluid (ISF) more accurately represents the environment around brain cells. This work therefore
117 focuses on brain-derived-vesicles (BD-EVs) in different tauopathies (AD, PSP, and certain forms of non-
118 hereditary frontotemporal lobar degeneration with Pick bodies [formerly known as PiD]) as well as non-demented
119 controls. The seeding ability from BD-EVs purified from both tau transgenic mice and patients with various
120 tauopathies is shown *in vitro*. In addition, AD BD-EVs are able to transmit tau pathology *in vivo* in a prion-like
121 process. These results highlight the importance of defining how the pathology propagates through the brain in
122 different tauopathies in order to design specific and tailored therapies as well as assessment tools for the evaluation
123 of clinical trials.

124

125
126
127
128
129
130
131
132
133
134
135
136
137
138
139
140
141
142
143
144
145
146
147
148
149
150
151
152
153
154

Results

In the present work, we isolated vesicles from the post-mortem BD-fluid of patients with various tauopathies, and we evaluated whether they contain species that are able to seed and spread the tau pathology in the brain.

EVs are present in the BD-fluid of a transgenic mouse model of tauopathy- To address this issue, we first isolated and characterized murine BD-EVs from a transgenic mouse model of tauopathy, the THY-tau30, that expresses human 1N4R tau protein with two pathogenic mutations (P301S and G272V) under the control of the neuron-specific Thy-1.2 promoter.^{44, 45} We prepared murine BD-fluids according to the protocol described by Polanco and collaborators.⁴⁶ We then purified and characterized vesicles from the murine BD-fluid using size-exclusion chromatography (SEC). As it is critical to remove any aggregated or macro-protein contaminants associated with the BD-EVs, we purified them using SEC rather than classical ultracentrifugation procedures.⁴⁷ The concentration and distribution of the vesicles were analyzed by a nanoparticle tracking analysis (NTA) system, the global protein content and its distribution were determined using UV detection or silver gel staining. SEC allowed us to efficiently enrich vesicles (fractions one to four [F1-4]) in our preparations from the protein contaminants, as previously described, while guaranteeing their morphological integrity (Figure 1C). A size distribution of the BD-EVs fractions revealed the presence of vesicles ranging from 50 nm to 400 nm (Figure 1D). Then, we used MALDI-TOF LC-MS/MS and quantitative analysis (IBAQ) to evaluate F1-4 proteomic content. We identified a total of 2064 proteins, of which 1635 (79%) are referenced in the VesiclePedia's database. Intensity-based absolute quantification (IBAQ scores) combined with Gene Ontology Cellular Components (GOCC) annotation revealed that GOCC terms associated with EVs represent 76% of total IBAQ scores for the 20 selected terms (Figure 1E). Among proteins recommended by the MISEV2018,⁴⁸ we identified a majority of categories 1a (non-tissue specific transmembrane or GPI-anchored proteins), 2a (cytosolic proteins recovered in EVs) and 4a (transmembrane, lipid-bound and soluble proteins associated to other intracellular compartments than plasma membrane/endosomes) (Figure 1F). Among them are found the cytosolic vesicular markers, HSP90 and tau protein (MAPT), which have been validated using either western-blot (Figure S1A) or ELISA assays (Figure 1G). In addition, using a proteinase K (PK) digestion assay, we showed that tau is found inside BD-EVs and not associated to their outer leaflet. Indeed, the extravesicular proteolysis (PK+, RIPA-) does not affect intravesicular tau concentration and thus confirming tau as an intravesicular component (Figure 1G). This full characterization

155 including NTA, silver gel staining, electron microscopy, proteomics and western-blot indicates that F1-4 contained
156 vesicles and are enriched in EVs. This pool was considered as the BD-EVs fraction in the following experiments.
157

158 **BD-EVs from a transgenic mouse model of tauopathy contain tau seeds-** In order to determine the role of EVs
159 in tau pathology spreading, the tau seeding content of BD-EVs prepared from 1-, 3- and 6-month-old THY-tau30
160 mice (a transgenic mouse model with progressive tau lesions) was evaluated.^{44, 45} As controls, we also isolated
161 BD-EVs from wild-type littermates and transgenic APP/PS1 mice (that develop amyloid deposition) that do not
162 exhibit tau aggregation.⁴⁹ Tau lesions were examined in the brains of these animals using two well characterized
163 anti-tau antibodies: MC1⁵⁰ (tau conformational dependent antibody) and AT100,⁵¹ (human phospho-dependent
164 antibody that allowed the detection of insoluble/aggregated tau. MC1 (Figure S2a-g) and AT100 (Figure S2h-n)
165 immunoreactivities were progressively detected in the hippocampal neurons of the CA1 layer of THY-tau30 mice
166 from 1 to 6 months. Whereas few to no MC1 (Figure S2e) and AT-100 (Figure S2l) immunoreactivities were seen
167 at 1-month-old respectively, MC1 immuno-positive neurites were easily detectable at 3 months with a few
168 positive cell bodies (Figure S2f). A very slight AT100-immunostaining was also seen in 3-month-old mice in the
169 subiculum (Figure S2m) when a strong immunoreactivity (in soma and neurites) was shown in 6-month-old
170 animals by both MC1 and AT100 antibodies (Figure S2g and n respectively). No AT100- and MC1-
171 immunoreactivities were observed in the wild-type littermates (Figure S2b-d, i-k) or in the transgenic APP/PS1
172 controls (Figure S2a, h). We then isolated vesicles of these murine BD-fluid and evaluated their ability to induce
173 a nucleation process using a biosensor assay.⁵² This involved a highly sensitive and quantitative assay using a
174 novel Fluorescence Resonance Energy Transfer (FRET)-based biosensor cell line that specifically reports tau
175 seeding activity. These cells express soluble forms of RD-P301Stau-CFP and RD-P301Stau-YFP. In presence of
176 seeds such as recombinant tau fibers, an oligomerization process allows energy transfer between CFP and YFP
177 that is detectable by flow cytometry. BD-EVs were introduced inside the biosensor cells using lipofectamine and
178 the seeding activity was quantified. BD-EVs of THY-tau30, unlike those obtained from the control lines (littermate
179 of THY-tau30 and APP/PS1), contained seed-competent species (Figure 2A). In fact, the FRET signal was
180 observed in an age-dependent manner only with THY-tau30 samples. The seeding effect was indeed related to
181 BD-EVs since their removal by ultracentrifugation in F1-4 abolished the FRET signal (compare ultracentrifugation
182 supernatant (no vesicle) to pellet (BD-EVs fraction)) (Figure 2B). In addition, tau was mainly found within vesicles
183 as demonstrated by tau immunodepletion after BD-EVs sonication (Figure 2C). The sonication procedure was

184 applied to ensure release of intravesicular tau and then facilitates its immunodepletion. Indeed, when intravesicular
185 tau was immunodepleted, a 70% decrease in the FRET signal was observed (Figure 2D).

186 Together, these data strongly support the hypothesis that the progressive appearance of tau pathology in mice leads
187 to the release of vesicles in the BD-fluid that contain seed-competent tau species.

188

189 **The seeding capacity of BD-EVs is heterogeneous among human tauopathies-** We showed that the presence
190 of tau seeds inside BD-EVs is related to the progression of tau pathology in the case of mice. Given the
191 heterogeneity among tauopathies, we questioned whether the seeding potential of BD-EVs would differ between
192 these neurodegenerative diseases. Post-mortem brain samples of human non-demented controls (n = 5), AD (n =
193 10), PSP (n = 10), and PiD (n = 5) patients were obtained (Table 1) in order to isolate BD-EVs, as described above
194 (Figure 1). Three brain regions (the prefrontal cortex, the occipital cortex, and the cerebellum) differentially
195 affected by the pathology were dissected, and tau lesions were quantified by immunohistochemistry (IHC) using
196 AT8, a phospho-dependent anti-tau antibody (Figures 3A and 3B). As expected, tau pathology is higher in AD
197 cases. After SEC purification, the BD-EVs shared the same characteristics (size, morphology, content) as those
198 isolated from the murine brain (Figure S3). Additionally, the presence of a specific transmembrane tetraspanins
199 associated with the vesicles was validated using immunogold electron microscopy (CD63; Figure S1B).

200 In contrast to the mice, where the whole brain was analyzed, only specific areas of the human brain were dissected
201 for BD-fluid isolation. To avoid any bias, the results were systematically normalized according to the weight of
202 the brain extracts used to prepare the BD-fluid. Our data showed that the vesicles concentration (Figure 4A) and
203 the global tau content (Figure 4B) did not differ among the tauopathies. Interestingly, BD-EVs from the brains of
204 the controls contained global tau at a similar level than from patients with tauopathies. This confirms that tau is
205 physiologically secreted in EVs and gives new insight into the mode of tau secretion in human brain.

206 To determine whether the tau protein present in BD-EVs can induce a nucleation process and whether this is
207 similar among tauopathies, BD-EVs were applied to biosensor cells, as before. The vesicular contents from the
208 prefrontal and occipital regions of the AD BD-fluid induced a significant FRET signal compared to the non-
209 demented controls. For BD-EVs from the PSP and PiD patients, a weak FRET signal was observed (Figure 4C),
210 which was consistent with neuropathology (Figure 3). It is relevant to note that among the PiD samples, one had
211 BD-EVs displaying a high FRET signal. This patient exhibited, in addition to Pick bodies, neurofibrillary tangles
212 (NFT) as seen in AD patients (Table 1), which could potentially account for this finding. Whereas the FRET signal
213 is related to the tau lesions in most cases (compare Figures 3B and 4C), as shown for the mice, the FRET signal

214 for the AD cerebellum was significantly higher than in the controls, even though both were devoid of tau lesions.
215 This FRET signal did not reflect a passive release of intracellular vesicles due to cell death, as there was no
216 correlation between the post-mortem delay and the FRET signal (Figure 4D). Together, our results demonstrate
217 that although the global level of tau is similar in BD-EVs, the seeding/nucleation competency is clearly different
218 according to the tauopathy considered, with a particularly high activity found in AD, in accordance with previous
219 studies.³¹

220

221 **BD-EVs are able to transmit tau pathology *in vivo***- To validate the seeding capacity of BD-EVs and to
222 determine whether these vesicles are able to transmit tau pathology *in vivo*, we adapted our *in vivo* model of
223 seeding.⁵³ This model is based on the intracerebral injection of material derived from AD brains into the
224 hippocampi of 1-month-old THY-tau30 mice. At this age, the endogenous tau pathology is very weak,⁴⁴ thus
225 allowing us to evaluate the seeding activity associated with the injected, human-derived material.

226 Four prefrontal cortex BD-fluid samples were pooled for each group: AD, PSP, PiD, and control. The BD-EVs
227 were tested using the FRET assay (Figure 5A) before being injected into the animals (6×10^9 vesicles per
228 hippocampus). A lower signal was generated for the PSP and PiD groups compared to the AD group, thus
229 confirming what was previously shown *in vitro* (Figure 4C). These intact BD-EVs were then bilaterally injected
230 in THY-tau30 mice and control littermates. Their respective ability to seed endogenous tau was monitored by IHC
231 using MC1 (tau conformational dependent antibody) or AT100 (human phospho-dependent antibody that allowed
232 the detection of insoluble/aggregated tau) (Figure 5B). When the BD-EVs were injected into the wild-type mice,
233 no MC1 or AT100 immunoreactivity was observed. No seeding occurred and the tau species contained within the
234 vesicles were not detected. In contrast, tau seeding was seen when BD-EVs from AD patients were injected in the
235 THY-tau30 mice. MC1- and AT100- immunoreactivities were quantified. In contrast, injected BD-EVs from PSP
236 and PiD did not induce any higher MC1- or AT100-immunoreactivity than BD-EVs purified from human control
237 brains (Figure 5C and D respectively). This lower seeding capacity of BD-EVs from PSP and PiD than those from
238 AD confirmed our *in vitro* data (Figure 4).

239 Altogether, our data show that BD-EVs containing tau seeds are then capable to mediate the misfolding and
240 phosphorylation of tau. It then strongly suggests the ability of the vesicular content to recruit and convert
241 endogenous tau into an abnormal conformational form differs among tauopathies, consistently with
242 neuropathology, thus suggesting the existence of specific species inside the BD-EVs according to the particular
243 tauopathy.

244

245 **Discussion-**

246

247 In this study, we investigated the role of BD-EVs in the heterogeneity and cell vulnerability of tauopathies. EVs
248 possess ligands and/or receptors that are compatible with a specific cell type, this could explain the neuronal
249 selectivity and the hierarchy of neurodegeneration within tauopathies. To date, most studies have investigated the
250 role of EVs in cell or animal models,^{26, 32, 46, 55, 56} but little data is available for humans, especially when considering
251 the ISF that is in direct contact with the brain cells and which is likely to be part of the prion-like process. The
252 presence of EVs capable of transferring material between cells (Figures 5 and Figure S4)^{31, 54} can help to explain
253 the progression of the pathology in tauopathies. A very recent and elegant study carried out by Ruan and
254 collaborators showed for the first time that AD brain-derived EVs spread tau pathology with defined interneurons
255 as their target.³¹ Here, we go further into this mechanism by determining the contribution of vesicles to the
256 heterogeneity of tauopathies by isolating and comparing BD-EVs from AD, PSP, and PiD, and from various brain
257 regions differentially affected by the tau pathology.

258 Using our mouse models, we were able to (1) control the quality of BD-EVs preparations, (2) demonstrate the role
259 of BD-EVs-tau in the seeding process, and most importantly, (3) highlight a link between BD-EVs seeding
260 capacity and the severity of the tau pathology. We confirmed these results in humans using brain regions that are
261 differentially affected by the pathology (the prefrontal cortex, the occipital cortex, and the cerebellum), and the
262 BD-EVs seeding capacity was particularly striking in the case of AD. Specifically, BD-EVs from AD patients
263 clearly contained seed-competent tau species (shown in the FRET assay), whereas such tau species were lower in
264 the PSP and PiD materials. In general, tau pathology is much weaker in PSP and PiD than in AD, and this may
265 participate to the low seeding capacity of vesicles in these pathologies. However, other explanations are also
266 possible: (1) although not unanimous, the prion-like propagation hypothesis may not be appropriate for PSP and
267 PiD,³ (2) a prion-like propagation may also exist for PSP and PiD, but EVs may not be the preferred shuttle,
268 contrary to AD, and (3) the FRET assay to measure seeding in PSP and PiD was less effective than in AD. In line
269 with this latter possibility, previous studies found that PSP materials gave heterogeneous FRET signals.^{33, 57}
270 Although a FRET signal was previously reported in PiD,³³ we did not observe a strong signal for most of the PiD
271 cases in the present work. In fact, the only PiD patient showing a FRET signal also displayed NFT, and this was
272 the oldest PiD patient. We previously published that PiD patients displaying Pick bodies with additional NFT have
273 aging/AD-like materials, namely a pathological tau triplet revealed by immunoblotting.^{58, 59} The presence of such
274 AD-like materials in this PiD patient could explain the high FRET signal as observed in the AD group.

275 Overall, our results suggest that the species shuttled by BD-EVs are very heterogeneous among tauopathies. What
276 do we know about tauopathies? In PiD, there is an accumulation of tau3R in Pick's bodies, and it is currently
277 classified as frontotemporal lobar degeneration (FTLD)-tau.⁶⁰ Nevertheless, it is difficult to differentiate PiD and
278 FTLD-tau with MAPT mutations (former FTDP-17). Both disorders have Pick bodies, but it has been shown that
279 the Pick bodies are pS262-negative in PiD,^{61, 62} and immunoreactive in FTLD-tau with MAPT mutations.^{63, 64} In
280 any case, this lesion would appear to be particularly harmful because PiD often affects people who are relatively
281 young (around 50 years of age), and it is characterized by very severe frontotemporal atrophy that is associated
282 with neuronal death. Pick bodies are mostly found in layers II and VI of the fronto-temporal isocortex and in the
283 granular cell layer of the dentate gyrus.^{59, 65} These cells mainly express 3R-tau isoforms. It can therefore be
284 postulated that these 3R-positive cells are fragile,⁶⁶ or else that the 3R-tau isoforms are more harmful than
285 propagative.⁶⁷⁻⁶⁹ In PSP, tau4R isoforms mostly aggregate to cause neurofibrillary degeneration. It is possible that
286 the 4R-tau variants are secreted and captured by the glia. In line with this, both PSP and corticobasal degeneration
287 are also characterized by gliofibrillary lesions.^{60, 70, 71} Finally, in AD, all six tau isoforms aggregate, and
288 neurofibrillary degeneration progresses in a hierarchical pathway from limbic, polymodal association, unimodal
289 association regions to the entire cerebral cortex. These observations suggest that tau seeds circulate in the ISF of
290 AD brains. Our data support this hypothesis since tau seeds were identified in circulating EVs in all brain areas
291 studied, even those devoid of tau lesions, such as the cerebellum. Depending on the brain area, EVs receptor/ligand
292 bearing cells may or may not be present, which explains why some regions are affected by pathology while others
293 are not. The combination of tau seeds in EVs and their ligand/receptor composition may therefore explain the
294 neuronal selectivity/vulnerability and hierarchical pathway of neurodegeneration among tauopathies.

295 The molecular species involved in the pathological cycle of cell-to-cell transmission remain unknown, even though
296 a great deal of work has been done to examine the roles of phosphorylation, truncation, oligomers, high molecular
297 weight species, etc.²⁹ Nevertheless, our work highlights the diversity of tau species inside BD-EVs among
298 tauopathies, and reinforces the hypothesis of prion-like propagation. It supports a trans-cellular transmission
299 mechanism with a specificity that could explain the hierarchical and stereotypical propagation compatible with the
300 Braak stages in AD.

301 Together, our data strongly support the existence of various tau species or co-factors inside BD-EVs among
302 tauopathies, and their identification is now necessary in order to be able to determine the mechanism of tau
303 pathology progression in these different diseases. The study raises a number of questions about therapeutic
304 strategies, such as immunotherapy, that target free extracellular tau. Deciphering the nature of the pathological

305 seeds found in the vesicles isolated from human brains, as well as the characteristics of the cargos/shuttles, will
306 help in the design of specific tools aiming to block tau spreading.
307

308
309
310
311
312
313
314
315
316
317
318
319
320
321
322
323
324
325
326
327
328
329
330
331
332
333
334
335
336
337
338

Materials and methods

Antibodies- The following antibodies were used for IHC, biochemical assays, and electron microscopy at the dilutions indicated below. Monoclonal antibody (mAb) AT8 recognizes the phosphoserine 202, phosphoserine 208, and phosphothreonine 205 residues of tau (MN1020; Thermo Scientific, Illkirch, France; 1/500 for IHC).⁷² The mAb MC1 (a generous gift from Dr. Peter Davis; 1/1000 for IHC) recognizes conformational changes, and its reactivity depends on both the N terminus (amino acids 7–9) and an amino acid sequence of tau (amino acids 313–322) in the third microtubule binding domain.^{50, 73} The mAb AT100 (MN1060; Thermo Scientific, Illkirch, France; 1/500 for IHC) recognizes phosphothreonine 212 and phosphoserine 214 and allowed the detection of insoluble/aggregated tau.^{51, 74-76} The mAb HT7 (MN100; Thermo Scientific, Illkirch, France; used in the INNOTEST® hTAU, as recommended by the manufacturer, Fujirebio) recognizes human tau (amino acids 159-163). Anti-HSP 90 α/β (F-8; sc-13119; 1/100 for western blotting). Anti-CD63 is a mouse mAb (Novusbio H5C6; nbp2-42225; 1/50 for electron microscopy), Anti-NeuN is a rabbit mAb (Chemicon MAB377; 1:1000), and anti-V5 is a mouse mAb (Millipore AB3792; 1:500).

Animals and human samples- The study was performed in accordance with the ethical standards laid down in the 1964 Declaration of Helsinki and its later amendments. The experimental research was performed with the approval of an ethics committee (agreement APAFIS#2264-2015101320441671 from CEEA75, Lille, France) and follows European guidelines for the use of animals. The animals (males and females) were housed in a temperature-controlled room (20-22°C) and maintained on a 12 h day/night cycle with food and water provided ad libitum in a specific, pathogen-free animal facility (with 5 mice per cage or 4 rats per cage). Animals were randomly allocated to the different experimental groups. THY-tau30 mice were used that express human 1N4R tau protein with two pathogenic mutations (P301S and G272V) under the control of the neuron-specific Thy-1.2 promoter.^{44, 45}

Non-demented human control (n=5), AD (n=10), PSP (n=10), and PiD (n=5) brain extracts were obtained from the Lille Neurobank (fulfilling French legal requirements concerning biological resources and declared to the competent authority under the number DC-2008-642) with donor consent, data protection, and ethics committee approval. Samples were managed by the CRB/CIC1403 Biobank, BB-0033-00030. The demographic data are listed in table 1.

339 **Cell culture-** The TauRDP301SFRET Biosensor cells (ATCC CRL-3275), HEK293T cells, and HeLa cells were
340 cultivated in Dulbecco's modified Eagle's medium with 10% fetal bovine serum, 1% GlutaMAX, and without
341 HEPES. The cells were maintained in a humidified incubator with 5% CO₂. All cell lines were passaged twice a
342 week. Rat primary cortical neurons were prepared from 17-day-old Wistar rat embryos, as previously described.⁷⁷
343 Ten days later, cells were infected with lentiviral vectors (LV) encoding human 1N4R wild-type Tau, as previously
344 described.⁷⁸

345

346 **Brain-derived fluid isolation-** BD-fluids were isolated, as previously described.⁴⁶ For the frozen human brains,
347 specific regions were removed (prefrontal cortex, occipital cortex, and cerebellum). 85 samples were used with a
348 mean of 1.5 g \pm 0.07 of tissue. Some brain areas were no more available: cerebellum (1AD, 1 PiD and 2 PSP),
349 cortex prefrontal (1 PSP). To avoid any bias in our results, normalization according to the weight of the brain
350 extracts have been systematically done.

351 For the mice, immediately after death, the whole brain (without the olfactory bulb and cerebellum) was recovered
352 and frozen. The tissues were incubated on ice in 5 ml of Hibernate-A (50 mM NaF, 200 nM Na₃VO₄, 10 nM
353 protease inhibitor [E64 from Sigma and Protease Inhibitor Cocktail from Roche]). The tissues were gently mixed
354 in a Potter homogenizer and 2 ml of 20 units/ml papain (LS003119, Worthington) in Hibernate-A were added to
355 the homogenate for 20 min at 37°C with agitation. 15 ml of cold Hibernate-A buffer was then added and mixed
356 by pipetting to stop the enzymatic activity. Successive centrifugations were applied at 4°C (300, 2000, and 10 000
357 g) to remove cells, membranes, and debris, respectively. The final supernatant was kept at -80°C before the BD-
358 EVs isolation procedures were applied.

359

360 **BD-EVs isolation-** The procedures to isolate the BD-EVs from the murine or human BD-fluid were carried out in
361 accordance with the MISEV guidelines that were established and updated in 2018 by the International Society for
362 Extracellular Vesicles.⁴⁸ We applied various controls to validate the enrichment and the content of the BD-EVs,
363 as recommended in these guidelines. However, the procedure described above to recover BD-fluids may lead to
364 cell lysis. The presence of intraluminal vesicles in our preparations can't be exclude. We thus consider that our
365 fractions are not pure but rather enriched in EVs and so refer as BD-EVs. 500 μ l of BD-fluid were loaded on the
366 top of a SEC column (10 ml column, CL2B sepharose, pore size 75 nm, Millipore)⁷⁹. It allowed us to recover a
367 mean of 7.94x10¹⁰ vesicles/g of tissue \pm 3.36x10⁹ in F1-F4 fractions (n=85 samples). Isolation was carried out
368 in phosphate buffered saline (PBS) with a flow of 36-48 sec/ml. The first 3 ml were eliminated and the following

369 20 fractions were recovered (with 500 µl per fraction). NTAs were performed on individual fractions diluted in
370 PBS with a Nanosight NS300 (Malvern Panatycal). To generate statistical data, five videos of 90 seconds were
371 recorded and analyzed using NTA software (camera level: 15; detection threshold: 4). When indicated a further
372 ultracentrifugation (100000g, 50 min at 4°C, TLA110 rotor) was done.

373

374 **Electron microscopy-** Fractions one to four from the SEC were pooled and concentrated to a final volume of 50
375 µl using Amicon® Ultra 3K (Merck Millipore). Samples (5 µl) were deposited on a carbon film supported grid
376 (400 mesh) and incubated at room temperature (RT) for 20 min. For immunogold labelling, fixation in 2%
377 paraformaldehyde (PFA; PO4 buffer 0.1 M, pH 7.4) was performed for 20 min. Grids were rinsed for 2-3 min in
378 PBS-Glycine (50 mM) at RT. They were then soaked in a mixture containing 1% PBS-Bovine serum albumin
379 (BSA) and 1% normal goat serum for 1h at RT before incubation with the primary Ab (1/50) in a mixture of 1%
380 PBS-BSA and 1% normal goat serum, followed by rinsing in 0.1% PBS-BSA. Grids were then incubated for 1h
381 at RT with the appropriate goat anti-mouse secondary Ab (1/20, 12 nm colloidal gold) and finally washed in PBS.
382 For immunogold labelling and morphological analyses, the grids were fixed in PBS-Glutaraldehyde (1%) for 5
383 min at RT and then rinsed in distilled water. They were incubated for 5 min in 1% uranyl acetate and for 10 min
384 on ice in a mixture containing 1% uranyl acetate/2% methylcellulose. Dry grids were observed under a
385 transmission electron microscope (Zeiss EM900).

386

387 **MALDI-TOF LC-MS/MS analysis- Protein Digestion-** F1-4 fractions were digested according to a modified
388 version of the iST method⁸⁰ (named miST method). Briefly, 50 µl solution in PBS were supplemented with in 50
389 µl miST lysis buffer (1% Sodium deoxycholate, 100 mM Tris pH 8.6, 10 mM DTT) and heated at 95°C for 5 min.
390 Samples were then diluted 1:1 (v:v) with water and reduced disulfides were alkylated by adding ¼ vol of 160 mM
391 chloroacetamide (final 32 mM) and incubating at 25°C for 45 min in the dark. Samples were adjusted to 3 mM
392 EDTA and digested with 0.5 µg Trypsin/LysC mix (Promega #V5073) for 1h at 37°C, followed by a second 1h
393 digestion with a second and identical aliquot of proteases. To remove sodium deoxycholate and desalt peptides,
394 two sample volumes of isopropanol containing 1% TFA were added to the digests, and the samples were desalted
395 on a strong cation exchange (SCX) plate (Oasis MCX; Waters Corp., Milford, MA) by centrifugation. After
396 washing with isopropanol/1%TFA, peptides were eluted in 250 µl of 80% MeCN, 19% water, 1% (v/v) ammonia;
397 **Liquid Chromatography-tandem Mass spectrometry-** Eluates after SCX desalting were frozen, dried, and
398 resuspended in variable volumes of 0.05% trifluoroacetic acid, 2% acetonitrile to equilibrate concentrations.

399 Approximately 1 µg of each sample was injected on column for nanoLC-MS analysis; **MS analysis- Data-**
400 dependent LC-MS/MS analysis of TMT sample was carried out on a Fusion Tribrid Orbitrap mass spectrometer
401 (Thermo Fisher Scientific) interfaced through a nano-electrospray ion source to an Ultimate 3000 RSLCnano
402 HPLC system (Dionex). Peptides were separated on a reversed-phase custom packed 40 cm C18 column (75 µm
403 ID, 100Å, Reprosil Pur 1.9 µm particles, Dr. Maisch, Germany) with a 4-76% acetonitrile gradient in 0.1% formic
404 acid (total time 140 min). Full MS survey scans were performed at 120'000 resolution. A data-dependent
405 acquisition method controlled by Xcalibur 4.2 software (Thermo Fisher Scientific) was used that optimized the
406 number of precursors selected (“top speed”) of charge 2+ to 5+ while maintaining a fixed scan cycle of 1.5s. The
407 precursor isolation window used was 0.7 Th. Full survey scans were performed at a 120'000 resolution, and a top
408 speed precursor selection strategy was applied to maximize acquisition of peptide tandem MS spectra with a
409 maximum cycle time of 0.6s. HCD fragmentation mode was used at a normalized collision energy of 32%, with a
410 precursor isolation window of 1.6 m/z, and MS/MS spectra were acquired in the ion trap. Peptides selected for
411 MS/MS were excluded from further fragmentation during 60s; **MS Data analysis-** Tandem MS data were
412 processed by the MaxQuant software (version 1.6.3.4)⁸¹ incorporating the Andromeda search engine⁸². The
413 UniProt reference proteome (RefProt) databases for Homo sapiens and mouse were used, supplemented with
414 sequences of common contaminants. Trypsin (cleavage at K, R) was used as the enzyme definition, allowing 2
415 missed cleavages. Carbamidomethylation of cysteine was specified as a fixed modification. N-terminal acetylation
416 of protein and oxidation of methionine were specified as variable modifications. All identifications were filtered
417 at 1% FDR at both the peptide and protein levels with default MaxQuant parameters⁸³. MaxQuant data were
418 further processed with Perseus software⁸⁴, R statistical software and Microsoft Excel. We considered proteins as
419 present in sample when unique + Razor Peptide Score >2 and an MS/MS Count >2. IBAQ values were calculated
420 based on the summed intensities of all unique peptides for a protein divided by the number of theoretical tryptic
421 peptides between 6 and 30 amino acids in length⁸⁵.

422

423 **Western blotting & silver gel staining-** Western blotting was performed, as previously described.⁸⁶ Briefly,
424 boiled samples (10 min, 100°C) were loaded onto a 4-12% Bis-Tris NuPAGE® Novex® gel (Invitrogen), followed
425 by transfer onto a 0.45 µm membrane, using the Novex system from Life Technologies (XCell II™ blot module).
426 The membrane was then incubated with blocking solution for 1h at RT before incubation with the appropriate
427 primary Ab overnight at 4°C. The membrane was then incubated for 1h with the appropriate secondary Ab (HRP
428 conjugated Ab, 1/50 000). The signal was visualized using enhanced chemiluminescence western blotting

429 detection reagents (GE Healthcare). For silver gel staining, the same procedure was followed without the transfer
430 onto a membrane. The gel was fixed overnight after migration in a mixture containing 40% ethanol and 10% acetic
431 acid. Proteins were revealed by silver staining using the PlusOne silver staining kit and following the
432 manufacturer's procedures (GE Healthcare).

433

434 **Tau immunodepletion-** BD-EVs fractions were isolated from the BD-fluid of 3-months-old THY-tau30.
435 Immunodepletion of tau from fractions 1-4 was performed using Magna CHIP Protein A+G magnetic beads (#16-
436 663, Sigma-Aldrich). After 30 min in water bath sonicator, fractions 1-4 were incubated overnight with 2 µg of
437 anti-tau Ab (HT7, #MN1000, Thermo Scientific) or control mouse monoclonal IgG1 antibody (GST [B-14]), Santa
438 Cruz) with rotation at 4°C. 20 µL of magnetic beads was incubated with the complex antibody-antigen for 2 hours
439 with rotation at 4°C. Magnetic beads-antibody-antigen complex was isolated using a magnetic holder and the
440 supernatant was collected.

441

442 **PK treatment-** PK assay was done as previously described.^{31, 54} BD-EVs (lysis or not with RIPA buffer) were
443 incubated with 10 µg/mL of PK 30 min at 37°C to remove extravesicular proteins. The PK activity was then
444 inhibited by adding 5 mM phenylmethylsulphonyl fluoride (PMSF) for 10 min at room temperature.

445

446 **Recombinant K18 fibrils-** The tau K18 recombinant protein and heparin were mixed to a ratio of 4:1 in
447 aggregation buffer (Hepes 10 mM, pH 6.9; NaCl 1000 mM) with a final protein concentration of 8 µM and
448 incubated for 36 to 48 hours at 37°C without shaking. The aggregation was confirmed at the end of the experiment
449 by adding 50 µM of Thioflavin T to a 100 µl aliquot and comparing this to a negative control without the addition
450 of heparin. The thioflavin T emission was detected at 490 nm after excitation at 440 nm using a PHERAstar (BMG
451 LABTECH GmbH, Ortenberg, Germany).

452

453 **FRET assay-** Cells were plated into a 12-wells plate (150 000 cells per well) 24 hours before treatment. Sonicated
454 K18 fibrils (2 µM) were used as a positive control and PBS was the negative control. BD-EVs fractions were
455 pooled (F1-F4) and concentrated in Amicon-3K columns to generate a final volume of 50 µl. The transfection
456 mixture (50 µl EVs + 50 µl optiMEM plus 10 µl of lipofectamine-2000 + 90 µl optiMEM) was incubated for 20
457 min at RT and added to the cells. After 72 hours, the cells were removed by scraping, and cell death was evaluated
458 by adding Zombie NIR™ for 30 min at RT (as recommended by the manufacturer of the Zombie NIR™ fixable

459 viability kit; BioLegend, 1/200). After one rinse in PBS, cells were fixed in 2% PFA for 10 min at RT and finally
460 suspended in PBS for cytometry analyses using the flow cytometer Aria SORP BD Biosciences (acquisition
461 software FACS DIVA V7.0 BD Biosciences) with the following excitation/emission wavelengths: excitation 405
462 nm-CFP emission 466+/-40 nm and FRET YFP 529+/-30 nm; excitation 488nm-YFP emission 529+/-30 nm. The
463 FRET data were quantified using the KALUZA Analysis Software v2. Results were expressed as the percentage
464 of FRET positive cells x MFI (median fluorescence intensity). For the human brain samples, this value was
465 normalized according to the weight of the tissue used to prepare the BD-fluid (percentage of FRET positive cells
466 x MFI/g of tissue).

467

468 **Stereotaxic injections-** Four BD-fluids (500 µl) were pooled for each of the AD, PSP, PiD, and control groups
469 (Table 1, bold), and the vesicles were isolated and concentrated to a final volume of 150 µl, as described above.
470 For each of these, 2 µl (6×10^9 vesicles) were bilaterally injected into the hippocampi of 1-month-old, anesthetized
471 (100 mg/kg ketamine, 20 mg/kg xylazine) THY-tau30 mice and littermates (n = 5 per group; weight = 15-20g), as
472 done previously (anterior-posterior: -2.5 mm; medial-lateral: +/- 1 mm; dorsal-ventral: -1.8 mm to bregma)⁵³. The
473 standard injection procedure involved the delivery of BD-EVs into THY-tau30 using a 10 µl Hamilton glass
474 syringe with a fixed needle. After injection at a rate of 0.25 µl per minute, the needle was left in place for 5 minutes
475 before removal to prevent any leakage of the injected material. For the experiments performed in rats (Figure S2),
476 3-months-old animals were anesthetized by intraperitoneal injection of a mixture of 100 mg/kg ketamine (Ketasol,
477 Graeb, Bern, Switzerland) and 10 mg/kg xylazine (Rompun, Bayer Health Care, Uznach, Switzerland). The
478 animals were bilaterally injected with 3 µl of BD-EVs into the dorsal dentate gyrus (anterior-posterior: -3 mm,
479 medial-lateral: +/- 2.5 mm, dorsal-ventral: -3.4 mm to bregma). The vesicles were injected at a rate of 0.2 µl per
480 minute and the needle was left in place for 5 minutes. In contrast to FRET assay, in all *in vivo* experiments, intact
481 BD-EVs were stereotactically injected without any lipofectamine.

482

483 **Tissue processing, IHC, and immunofluorescence-** For the human brains, the different cerebral regions (the
484 prefrontal cortex, the occipital cortex, and the cerebellum) were dissected, and the tau lesion quantification was
485 performed using the mirror zones. For the mice, the whole brains were dissected and the tau lesions were quantified
486 using dedicated mice. For the human brain sections, automated IHC was performed using 4-µm-thick formalin-
487 fixed, paraffin-embedded (FFPE) tissue on a BenchMark Ultra (Roche tissue diagnostics[®]) with the UltraView
488 DAB IHC Detection Kit (Ventana[®]) and the primary Ab AT8 (1:500). For the THY-tau30 and littermate mice, at

489 4 weeks post-injection they were deeply anesthetized and transcardially perfused with ice-cold 0.9% saline
490 solution and subsequently with 4% PFA for 10 minutes. The brains were immediately removed, fixed overnight
491 in 4% PFA, washed in PBS, placed in 20% sucrose for 24h, and frozen until further use. Free-floating coronal
492 sections (40 μm thickness) were obtained using a cryostat microtome. For IHC, the brain sections were washed in
493 PBS-0.2% Triton X-100, treated for 30 minutes at RT with 0.3% H_2O_2 , and then washed three times. Non-specific
494 binding was blocked using a 'Mouse on Mouse' reagent (1:100 in PBS, Vector Laboratories) for 60 minutes at
495 RT. After three rinses in PBS-0.2% Triton X-100, the sections were incubated with the primary Ab MC1 (1:1000)
496 or AT100 (1:500) in PBS-0.2% Triton X-100 (1:1000) overnight at 4°C. After three rinses in PBS-0.2% Triton X-
497 100, labelling was amplified by incubation with an anti-mouse biotinylated IgG (1:400 in PBS-0.2% Triton X-
498 100, Vector Laboratories) for 60 minutes at RT. This was followed by a 120-minute application of the avidin-
499 biotin-HRP complex (ABC kit, 1:400 in PBS, Vector Laboratories) prior to the addition of diaminobenzidine
500 tetrahydrochloride (Vector Laboratories) in Tris-HCl 0.2 mol/l, pH 7.6, containing 0.0015% of H_2O_2 for
501 visualization. Brain sections were then mounted, air-dried, dehydrated by passage through a graded series of
502 alcohol (30%, 70%, 95%, 100%) and toluene baths, and finally mounted with Vectamount (Vector Laboratories).
503 For the rats, three weeks after the BD-EVs injections, they were deeply anesthetized and transcardially perfused
504 with 4% PFA. A series of one-in-six 30- μm -thick coronal sections were prepared and incubated at 4°C for 24
505 hours in PBS containing 0.3% Triton-X100 with the following primary Ab: rabbit anti-NeuN and mouse anti-V5.
506 After several rinses with PBS, the sections were incubated for 90 minutes at RT in a PBS solution containing a
507 mixture of the appropriate secondary Ab: Alexa-488 and Alexa-555 mouse secondary antibodies (1:500, Life
508 Technologies). All of the sections were counterstained for 10 minutes with DAPI (4',6-Diamidino-2-Phenylindole;
509 Merck; 1:5,000 dilution) to label the nuclei. IHC against V5/NeuN was followed by a final autofluorescence
510 elimination step. To this end, Autofluorescence Eliminator reagent (EMD Millipore, 2160) was used, according
511 to the manufacturer's instructions. Samples were mounted in VECTASHIELD. Images were acquired (series of
512 50-75 multiple optical sections, $z = 0.2 \mu\text{m}$) with a Zeiss LSM 880 Quasar confocal system (63x + 4x numerical
513 zoom) equipped with Airyscan.

514

515 **Tau lesion quantification-** For blinded quantification of MC1 and AT100 immunoreactivity, the CA1 region of
516 the hippocampus was chosen as the quantification zone. We selected and quantified five brain sections covering
517 the entire hippocampus (bregmas -2.30 to -2.8) and manually counted the number of MC1 or AT100 positive
518 somas per brain section. Results were presented as the number of neurofibrillary tangle per brain section. Human

519 brain sections were blindly quantified using QuPath-0.2.1 software for the full mirror image of the paraffin-
520 embedded sections. Thresholds were established using a dedicated artificial intelligence algorithm (Artificial
521 Neuronal Network; ANN_MLP) with identified objects on a set of slides, and these segmentation thresholds
522 remained constant throughout the analyses. Results were expressed as a percentage of tau lesions ([AT8 positive
523 pixels/total pixels] x100).

524

525 **Statistical analyses-** Statistics and plots were generated using GraphPad Prism 8 software (version 8.0.0). The
526 normality of the distributions was assessed graphically and using the Shapiro-Wilk test. In the case of a non-
527 Gaussian distribution, the Mann-Whitney U-test was used for one-to-one comparison, and one-way non-
528 parametric ANOVAs (Kruskal-Wallis) with post-hoc test was used for multiple comparisons. In the case of
529 Gaussian distribution, one-way ANOVAs with post-hoc test was used for multiple comparisons. Data were
530 reported as the mean \pm standard deviation (SD). Correlation analyses were performed using a non-parametric
531 Spearman correlation test. The statistical tests adopted a two-tailed α level of 0.05.

532

533

534 **Acknowledgements-** This work was supported by grants from the program Investissement d'Avenir LabEx
535 (investing in the future laboratory excellence) DISTALZ (Development of Innovative Strategies for a
536 Transdisciplinary Approach to ALZheimer's disease), Fondation Alzheimer (project Ectausome), Fondation pour
537 la Recherche Médicale, ANR grants (GRAND, TONIC), and the PSP France Association. Our laboratories are
538 also supported by LiCEND (Lille Centre of Excellence in Neurodegenerative Disorders), CNRS, Inserm,
539 Métropole Européenne de Lille, the University of Lille, I-SITE ULNE, Région Hauts de France and FEDER. We
540 are grateful to the Lille Neurobank and Pr Claude-Alain Maurage for the access to the human brain samples. This
541 study was also supported by a Synapsis Foundation fellowship awarded to K.R. and the Lausanne University
542 Hospital (CHUV). The authors thank the Protein Analysis Facility of the University of Lausanne for their technical
543 support, in particular Dr. M. Quadroni. We also thank L. Culebras for help for circular graphical representation.
544 We are grateful to the UMS-2014 US41 PLBS for access to the confocal microscopy and flow cytometry core
545 facility Platform at the HU site of the BioImaging Center Lille for their help and for access to the cytometer. We
546 thank Peter Davies for providing the MC1 antibody. The authors report no competing interests.

547

548 **Author contributions-** M.C. and L.B. designed and conceptualized the study, wrote the original draft and then
549 reviewed the manuscript. E.L., K.R., N.D and N.T helped for the manuscript editing. E.L., R.P., R.C., S.L., T.B.,
550 S.B., V.D., A.L., S.S., C.D., J.E. and K.R. performed the experiments.

551

552 **References-**

553

- 554 1. Weingarten, MD, Lockwood, AH, Hwo, SY, and Kirschner, MW (1975). A protein factor essential for
555 microtubule assembly. *Proc Natl Acad Sci U S A* **72**: 1858-1862.
- 556 2. Spillantini, MG, and Goedert, M (2013). Tau pathology and neurodegeneration. *Lancet Neurol* **12**: 609-
557 622.
- 558 3. Colin, M, Dujardin, S, Schraen-Maschke, S, Meno-Tetang, G, Duyckaerts, C, Courade, JP, *et al.* (2020).
559 From the prion-like propagation hypothesis to therapeutic strategies of anti-tau immunotherapy. *Acta*
560 *Neuropathol* **139**: 3-25.
- 561 4. Falcon, B, Zhang, W, Schweighauser, M, Murzin, AG, Vidal, R, Garringer, HJ, *et al.* (2018). Tau
562 filaments from multiple cases of sporadic and inherited Alzheimer's disease adopt a common fold. *Acta*
563 *Neuropathol* **136**: 699-708.

- 564 5. Falcon, B, Zivanov, J, Zhang, W, Murzin, AG, Garringer, HJ, Vidal, R, *et al.* (2019). Novel tau filament
565 fold in chronic traumatic encephalopathy encloses hydrophobic molecules. *Nature* **568**: 420-423.
- 566 6. Fitzpatrick, AWP, Falcon, B, He, S, Murzin, AG, Murshudov, G, Garringer, HJ, *et al.* (2017). Cryo-EM
567 structures of tau filaments from Alzheimer's disease. *Nature* **547**: 185-190.
- 568 7. Duyckaerts, C, Bannicib, M, Grignon, Y, Uchihara, T, He, Y, Piette, F, *et al.* (1997). Modeling the
569 relation between neurofibrillary tangles and intellectual status. *Neurobiol Aging* **18**: 267-273.
- 570 8. Braak, H, and Braak, E (1991). Neuropathological staging of Alzheimer-related changes. *Acta*
571 *Neuropathol* **82**: 239-259.
- 572 9. Delacourte, A, David, JP, Sergeant, N, Buee, L, Wattez, A, Vermersch, P, *et al.* (1999). The biochemical
573 pathway of neurofibrillary degeneration in aging and Alzheimer's disease. *Neurology* **52**: 1158-1165.
- 574 10. Verny, M, Duyckaerts, C, Agid, Y, and Hauw, JJ (1996). The significance of cortical pathology in
575 progressive supranuclear palsy. Clinico-pathological data in 10 cases. *Brain* **119 (Pt 4)**: 1123-1136.
- 576 11. Williams, DR, Holton, JL, Strand, C, Pittman, A, de Silva, R, Lees, AJ, *et al.* (2007). Pathological tau
577 burden and distribution distinguishes progressive supranuclear palsy-parkinsonism from Richardson's
578 syndrome. *Brain* **130**: 1566-1576.
- 579 12. Saito, Y, Ruberu, NN, Sawabe, M, Arai, T, Tanaka, N, Kakuta, Y, *et al.* (2004). Staging of argyrophilic
580 grains: an age-associated tauopathy. *J Neuropathol Exp Neurol* **63**: 911-918.
- 581 13. Irwin, DJ, Bretschneider, J, McMillan, CT, Cooper, F, Olm, C, Arnold, SE, *et al.* (2016). Deep clinical
582 and neuropathological phenotyping of Pick disease. *Ann Neurol* **79**: 272-287.
- 583 14. Sotiropoulos, I, Galas, MC, Silva, JM, Skoulakis, E, Wegmann, S, Maina, MB, *et al.* (2017). Atypical,
584 non-standard functions of the microtubule associated Tau protein. *Acta Neuropathol Commun* **5**: 91.
- 585 15. Fontaine, SN, Zheng, D, Sabbagh, JJ, Martin, MD, Chaput, D, Darling, A, *et al.* (2016). DnaJ/Hsc70
586 chaperone complexes control the extracellular release of neurodegenerative-associated proteins. *EMBO*
587 *J* **35**: 1537-1549.
- 588 16. Kang, S, Son, SM, Baik, SH, Yang, J, and Mook-Jung, I (2019). Autophagy-Mediated Secretory Pathway
589 is Responsible for Both Normal and Pathological Tau in Neurons. *J Alzheimers Dis* **70**: 667-680.
- 590 17. Katsinelos, T, Zeitler, M, Dimou, E, Karakatsani, A, Muller, HM, Nachman, E, *et al.* (2018).
591 Unconventional Secretion Mediates the Trans-cellular Spreading of Tau. *Cell Rep* **23**: 2039-2055.
- 592 18. Lee, J, and Ye, Y (2018). The Roles of Endo-Lysosomes in Unconventional Protein Secretion. *Cells* **7**.

- 593 19. Merezhko, M, Brunello, CA, Yan, X, Vihinen, H, Jokitalo, E, Uronen, RL, *et al.* (2018). Secretion of Tau
594 via an Unconventional Non-vesicular Mechanism. *Cell Rep* **25**: 2027-2035 e2024.
- 595 20. Mohamed, NV, Desjardins, A, and Leclerc, N (2017). Tau secretion is correlated to an increase of Golgi
596 dynamics. *PLoS One* **12**: e0178288.
- 597 21. Pooler, AM, Phillips, EC, Lau, DH, Noble, W, and Hanger, DP (2013). Physiological release of
598 endogenous tau is stimulated by neuronal activity. *EMBO Rep* **14**: 389-394.
- 599 22. Rodriguez, L, Mohamed, NV, Desjardins, A, Lippe, R, Fon, EA, and Leclerc, N (2017). Rab7A regulates
600 tau secretion. *J Neurochem* **141**: 592-605.
- 601 23. Sato, C, Barthelemy, NR, Mawuenyega, KG, Patterson, BW, Gordon, BA, Jockel-Balsarotti, J, *et al.*
602 (2018). Tau Kinetics in Neurons and the Human Central Nervous System. *Neuron* **97**: 1284-1298 e1287.
- 603 24. Sayas, CL, Medina, M, Cuadros, R, Olla, I, Garcia, E, Perez, M, *et al.* (2019). Role of tau N-terminal
604 motif in the secretion of human tau by End Binding proteins. *PLoS One* **14**: e0210864.
- 605 25. Tang, Z, Ioja, E, Bereczki, E, Hultenby, K, Li, C, Guan, Z, *et al.* (2015). mTor mediates tau localization
606 and secretion: Implication for Alzheimer's disease. *Biochim Biophys Acta* **1853**: 1646-1657.
- 607 26. Perez, M, Avila, J, and Hernandez, F (2019). Propagation of Tau via Extracellular Vesicles. *Front*
608 *Neurosci* **13**: 698.
- 609 27. van Niel, G, D'Angelo, G, and Raposo, G (2018). Shedding light on the cell biology of extracellular
610 vesicles. *Nat Rev Mol Cell Biol* **19**: 213-228.
- 611 28. Maas, SLN, Breakefield, XO, and Weaver, AM (2017). Extracellular Vesicles: Unique Intercellular
612 Delivery Vehicles. *Trends Cell Biol* **27**: 172-188.
- 613 29. Pernegre, C, Duquette, A, and Leclerc, N (2019). Tau Secretion: Good and Bad for Neurons. *Front*
614 *Neurosci* **13**: 649.
- 615 30. Wang, YP, Biernat, J, Pickhardt, M, Mandelkow, E, and Mandelkow, EM (2007). Stepwise proteolysis
616 liberates tau fragments that nucleate the Alzheimer-like aggregation of full-length tau in a neuronal cell
617 model. *Proc Natl Acad Sci U S A* **104**: 10252-10257.
- 618 31. Ruan, Z, Pathak, D, Venkatesan Kalavai, S, Yoshii-Kitahara, A, Muraoka, S, Bhatt, N, *et al.* (2020).
619 Alzheimer's disease brain-derived extracellular vesicles spread tau pathology in interneurons. *Brain*.
- 620 32. Polanco, JC, Hand, GR, Briner, A, Li, C, and Gotz, J (2021). Exosomes induce endolysosomal
621 permeabilization as a gateway by which exosomal tau seeds escape into the cytosol. *Acta Neuropathol*.

- 622 33. Sanders, DW, Kaufman, SK, DeVos, SL, Sharma, AM, Mirbaha, H, Li, A, *et al.* (2014). Distinct tau
623 prion strains propagate in cells and mice and define different tauopathies. *Neuron* **82**: 1271-1288.
- 624 34. Dujardin, S, Commins, C, Lathuiliere, A, Beerepoot, P, Fernandes, AR, Kamath, TV, *et al.* (2020). Tau
625 molecular diversity contributes to clinical heterogeneity in Alzheimer's disease. *Nat Med* **26**: 1256-1263.
- 626 35. Saman, S, Kim, W, Raya, M, Visnick, Y, Miro, S, Jackson, B, *et al.* (2012). Exosome-associated tau is
627 secreted in tauopathy models and is selectively phosphorylated in cerebrospinal fluid in early Alzheimer
628 disease. *J Biol Chem* **287**: 3842-3849.
- 629 36. Spitzer, P, Mulzer, LM, Oberstein, TJ, Munoz, LE, Lewczuk, P, Kornhuber, J, *et al.* (2019).
630 Microvesicles from cerebrospinal fluid of patients with Alzheimer's disease display reduced
631 concentrations of tau and APP protein. *Sci Rep* **9**: 7089.
- 632 37. Muraoka, S, DeLeo, AM, Sethi, MK, Yukawa-Takamatsu, K, Yang, Z, Ko, J, *et al.* (2020). Proteomic
633 and biological profiling of extracellular vesicles from Alzheimer's disease human brain tissues.
634 *Alzheimers Dement* **16**: 896-907.
- 635 38. Fiandaca, MS, Kapogiannis, D, Mapstone, M, Boxer, A, Eitan, E, Schwartz, JB, *et al.* (2015).
636 Identification of preclinical Alzheimer's disease by a profile of pathogenic proteins in neurally derived
637 blood exosomes: A case-control study. *Alzheimers Dement* **11**: 600-607 e601.
- 638 39. Guix, FX, Corbett, GT, Cha, DJ, Mustapic, M, Liu, W, Mengel, D, *et al.* (2018). Detection of
639 Aggregation-Competent Tau in Neuron-Derived Extracellular Vesicles. *Int J Mol Sci* **19**.
- 640 40. Jia, L, Qiu, Q, Zhang, H, Chu, L, Du, Y, Zhang, J, *et al.* (2019). Concordance between the assessment of
641 Abeta42, T-tau, and P-T181-tau in peripheral blood neuronal-derived exosomes and cerebrospinal fluid.
642 *Alzheimers Dement* **15**: 1071-1080.
- 643 41. Mustapic, M, Eitan, E, Werner, JK, Jr., Berkowitz, ST, Lazaropoulos, MP, Tran, J, *et al.* (2017). Plasma
644 Extracellular Vesicles Enriched for Neuronal Origin: A Potential Window into Brain Pathologic
645 Processes. *Front Neurosci* **11**: 278.
- 646 42. Perrotte, M, Haddad, M, Le Page, A, Frost, EH, Fulop, T, and Ramassamy, C (2020). Profile of
647 pathogenic proteins in total circulating extracellular vesicles in mild cognitive impairment and during the
648 progression of Alzheimer's disease. *Neurobiol Aging* **86**: 102-111.
- 649 43. Winston, CN, Goetzl, EJ, Akers, JC, Carter, BS, Rockenstein, EM, Galasko, D, *et al.* (2016). Prediction
650 of conversion from mild cognitive impairment to dementia with neuronally derived blood exosome
651 protein profile. *Alzheimers Dement (Amst)* **3**: 63-72.

- 652 44. Leroy, K, Bretteville, A, Schindowski, K, Gilissen, E, Authelet, M, De Decker, R, *et al.* (2007). Early
653 axonopathy preceding neurofibrillary tangles in mutant tau transgenic mice. *Am J Pathol* **171**: 976-992.
- 654 45. Schindowski, K, Bretteville, A, Leroy, K, Begard, S, Brion, JP, Hamdane, M, *et al.* (2006). Alzheimer's
655 disease-like tau neuropathology leads to memory deficits and loss of functional synapses in a novel
656 mutated tau transgenic mouse without any motor deficits. *Am J Pathol* **169**: 599-616.
- 657 46. Polanco, JC, Scicluna, BJ, Hill, AF, and Gotz, J (2016). Extracellular Vesicles Isolated from the Brains
658 of rTg4510 Mice Seed Tau Protein Aggregation in a Threshold-dependent Manner. *J Biol Chem* **291**:
659 12445-12466.
- 660 47. Boing, AN, van der Pol, E, Grootemaat, AE, Coumans, FA, Sturk, A, and Nieuwland, R (2014). Single-
661 step isolation of extracellular vesicles by size-exclusion chromatography. *J Extracell Vesicles* **3**.
- 662 48. They, C, Witwer, KW, Aikawa, E, Alcaraz, MJ, Anderson, JD, Andriantsitohaina, R, *et al.* (2018).
663 Minimal information for studies of extracellular vesicles 2018 (MISEV2018): a position statement of the
664 International Society for Extracellular Vesicles and update of the MISEV2014 guidelines. *J Extracell*
665 *Vesicles* **7**: 1535750.
- 666 49. Jankowsky, JL, Slunt, HH, Ratovitski, T, Jenkins, NA, Copeland, NG, and Borchelt, DR (2001). Co-
667 expression of multiple transgenes in mouse CNS: a comparison of strategies. *Biomol Eng* **17**: 157-165.
- 668 50. Jeganathan, S, Hascher, A, Chinnathambi, S, Biernat, J, Mandelkow, EM, and Mandelkow, E (2008).
669 Proline-directed pseudo-phosphorylation at AT8 and PHF1 epitopes induces a compaction of the
670 paperclip folding of Tau and generates a pathological (MC-1) conformation. *J Biol Chem* **283**: 32066-
671 32076.
- 672 51. Allen, B, Ingram, E, Takao, M, Smith, MJ, Jakes, R, Virdee, K, *et al.* (2002). Abundant tau filaments and
673 nonapoptotic neurodegeneration in transgenic mice expressing human P301S tau protein. *J Neurosci* **22**:
674 9340-9351.
- 675 52. Holmes, BB, Furman, JL, Mahan, TE, Yamasaki, TR, Mirbaha, H, Eades, WC, *et al.* (2014). Proteopathic
676 tau seeding predicts tauopathy in vivo. *Proc Natl Acad Sci U S A* **111**: E4376-4385.
- 677 53. Albert, M, Mairet-Coello, G, Danis, C, Lieger, S, Caillierez, R, Carrier, S, *et al.* (2019). Prevention of
678 tau seeding and propagation by immunotherapy with a central tau epitope antibody. *Brain* **142**: 1736-
679 1750.
- 680 54. Wang, Y, Balaji, V, Kaniyappan, S, Kruger, L, Irsen, S, Tepper, K, *et al.* (2017). The release and trans-
681 synaptic transmission of Tau via exosomes. *Mol Neurodegener* **12**: 5.

- 682 55. Polanco, JC, Li, C, Durisic, N, Sullivan, R, and Gotz, J (2018). Exosomes taken up by neurons hijack the
683 endosomal pathway to spread to interconnected neurons. *Acta Neuropathol Commun* **6**: 10.
- 684 56. Winston, CN, Aulston, B, Rockenstein, EM, Adame, A, Prikhodko, O, Dave, KN, *et al.* (2019). Neuronal
685 Exosome-Derived Human Tau is Toxic to Recipient Mouse Neurons in vivo. *J Alzheimers Dis* **67**: 541-
686 553.
- 687 57. Kaufman, SK, Sanders, DW, Thomas, TL, Ruchinkas, AJ, Vaquer-Alicea, J, Sharma, AM, *et al.* (2016).
688 Tau Prion Strains Dictate Patterns of Cell Pathology, Progression Rate, and Regional Vulnerability In
689 Vivo. *Neuron* **92**: 796-812.
- 690 58. Buee Scherrer, V, Hof, PR, Buee, L, Leveugle, B, Vermersch, P, Perl, DP, *et al.* (1996).
691 Hyperphosphorylated tau proteins differentiate corticobasal degeneration and Pick's disease. *Acta*
692 *Neuropathol* **91**: 351-359.
- 693 59. Hof, PR, Bouras, C, Perl, DP, and Morrison, JH (1994). Quantitative neuropathologic analysis of Pick's
694 disease cases: cortical distribution of Pick bodies and coexistence with Alzheimer's disease. *Acta*
695 *Neuropathol* **87**: 115-124.
- 696 60. Forrest, SL, Kril, JJ, Stevens, CH, Kwok, JB, Hallupp, M, Kim, WS, *et al.* (2018). Retiring the term
697 FTDP-17 as MAPT mutations are genetic forms of sporadic frontotemporal tauopathies. *Brain* **141**: 521-
698 534.
- 699 61. Delacourte, A, Sergeant, N, Wattez, A, Gauvreau, D, and Robitaille, Y (1998). Vulnerable neuronal
700 subsets in Alzheimer's and Pick's disease are distinguished by their tau isoform distribution and
701 phosphorylation. *Ann Neurol* **43**: 193-204.
- 702 62. Mailliot, C, Sergeant, N, Bussiere, T, Caillet-Boudin, ML, Delacourte, A, and Buee, L (1998).
703 Phosphorylation of specific sets of tau isoforms reflects different neurofibrillary degeneration processes.
704 *FEBS Lett* **433**: 201-204.
- 705 63. Chaunu, MP, Deramecourt, V, Buee-Scherrer, V, Le Ber, I, Brice, A, Ehrle, N, *et al.* (2013). Juvenile
706 frontotemporal dementia with parkinsonism associated with tau mutation G389R. *J Alzheimers Dis* **37**:
707 769-776.
- 708 64. Deramecourt, V, Lebert, F, Maurage, CA, Fernandez-Gomez, FJ, Dujardin, S, Colin, M, *et al.* (2012).
709 Clinical, neuropathological, and biochemical characterization of the novel tau mutation P332S. *J*
710 *Alzheimers Dis* **31**: 741-749.

- 711 65. Buee, L, Bussiere, T, Buee-Scherrer, V, Delacourte, A, and Hof, PR (2000). Tau protein isoforms,
712 phosphorylation and role in neurodegenerative disorders. *Brain Res Brain Res Rev* **33**: 95-130.
- 713 66. Richetin, K, Steullet, P, Pachoud, M, Perbet, R, Parietti, E, Maheswaran, M, *et al.* (2020). Tau
714 accumulation in astrocytes of the dentate gyrus induces neuronal dysfunction and memory deficits in
715 Alzheimer's disease. *Nat Neurosci*.
- 716 67. Dujardin, S, Begard, S, Caillierez, R, Lachaud, C, Carrier, S, Lieger, S, *et al.* (2018). Different tau species
717 lead to heterogeneous tau pathology propagation and misfolding. *Acta Neuropathol Commun* **6**: 132.
- 718 68. Sealey, MA, Vourkou, E, Cowan, CM, Bossing, T, Quraishe, S, Grammenoudi, S, *et al.* (2017). Distinct
719 phenotypes of three-repeat and four-repeat human tau in a transgenic model of tauopathy. *Neurobiol Dis*
720 **105**: 74-83.
- 721 69. Xu, C, Guo, J, Li, L, Wang, X, Zhou, Q, Sun, D, *et al.* (2020). Co-Expression of Three Wild-Type 3R-
722 Tau Isoforms Induces Memory Deficit via Oxidation-Related DNA Damage and Cell Death: A Promising
723 Model for Tauopathies. *J Alzheimers Dis* **73**: 1105-1123.
- 724 70. Rosler, M, Retz, W, Retz-Junginger, P, and Dennler, HJ (1998). Effects of two-year treatment with the
725 cholinesterase inhibitor rivastigmine on behavioural symptoms in Alzheimer's disease. *Behav Neurol* **11**:
726 211-216.
- 727 71. Jadhav, S, Avila, J, Scholl, M, Kovacs, GG, Kovari, E, Skrabana, R, *et al.* (2019). A walk through tau
728 therapeutic strategies. *Acta Neuropathol Commun* **7**: 22.
- 729 72. Malia, TJ, Teplyakov, A, Ernst, R, Wu, SJ, Lacy, ER, Liu, X, *et al.* (2016). Epitope mapping and
730 structural basis for the recognition of phosphorylated tau by the anti-tau antibody AT8. *Proteins* **84**: 427-
731 434.
- 732 73. Jicha, GA, Bowser, R, Kazam, IG, and Davies, P (1997). Alz-50 and MC-1, a new monoclonal antibody
733 raised to paired helical filaments, recognize conformational epitopes on recombinant tau. *J Neurosci Res*
734 **48**: 128-132.
- 735 74. Hoffmann, R, Lee, VM, Leight, S, Varga, I, and Otvos, L, Jr. (1997). Unique Alzheimer's disease paired
736 helical filament specific epitopes involve double phosphorylation at specific sites. *Biochemistry* **36**: 8114-
737 8124.
- 738 75. Zheng-Fischhofer, Q, Biernat, J, Mandelkow, EM, Illenberger, S, Godemann, R, and Mandelkow, E
739 (1998). Sequential phosphorylation of Tau by glycogen synthase kinase-3beta and protein kinase A at

740 Thr212 and Ser214 generates the Alzheimer-specific epitope of antibody AT100 and requires a paired-
741 helical-filament-like conformation. *Eur J Biochem* **252**: 542-552.

742 76. Yoshida, H, and Goedert, M (2006). Sequential phosphorylation of tau protein by cAMP-dependent
743 protein kinase and SAPK4/p38delta or JNK2 in the presence of heparin generates the AT100 epitope. *J*
744 *Neurochem* **99**: 154-164.

745 77. Galas, MC, Dourlen, P, Begard, S, Ando, K, Blum, D, Hamdane, M, *et al.* (2006). The peptidylprolyl
746 cis/trans-isomerase Pin1 modulates stress-induced dephosphorylation of Tau in neurons. Implication in a
747 pathological mechanism related to Alzheimer disease. *J Biol Chem* **281**: 19296-19304.

748 78. Dujardin, S, Begard, S, Caillierez, R, Lachaud, C, Delattre, L, Carrier, S, *et al.* (2014). Ectosomes: a new
749 mechanism for non-exosomal secretion of tau protein. *PLoS One* **9**: e100760.

750 79. Hagel, L, Östberg, M, and Andersson, T (1996). Apparent pore size distributions of chromatography
751 media. *Journal of Chromatography A* **743**: 33-42.

752 80. Kulak, NA, Pichler, G, Paron, I, Nagaraj, N, and Mann, M (2014). Minimal, encapsulated proteomic-
753 sample processing applied to copy-number estimation in eukaryotic cells. *Nat Methods* **11**: 319-324.

754 81. Cox, J, and Mann, M (2008). MaxQuant enables high peptide identification rates, individualized p.p.b.-
755 range mass accuracies and proteome-wide protein quantification. *Nat Biotechnol* **26**: 1367-1372.

756 82. Cox, J, Neuhauser, N, Michalski, A, Scheltema, RA, Olsen, JV, and Mann, M (2011). Andromeda: a
757 peptide search engine integrated into the MaxQuant environment. *J Proteome Res* **10**: 1794-1805.

758 83. Baietti, MF, Zhang, Z, Mortier, E, Melchior, A, Degeest, G, Geeraerts, A, *et al.* (2012). Syndecan-
759 syntenin-ALIX regulates the biogenesis of exosomes. *Nat Cell Biol* **14**: 677-685.

760 84. Tyanova, S, Temu, T, Sinitcyn, P, Carlson, A, Hein, MY, Geiger, T, *et al.* (2016). The Perseus
761 computational platform for comprehensive analysis of (prote)omics data. *Nat Methods* **13**: 731-740.

762 85. Schwanhausser, B, Busse, D, Li, N, Dittmar, G, Schuchhardt, J, Wolf, J, *et al.* (2011). Global
763 quantification of mammalian gene expression control. *Nature* **473**: 337-342.

764 86. d'Orange, M, Auregan, G, Cheramy, D, Gaudin-Guerif, M, Lieger, S, Guillemier, M, *et al.* (2018).
765 Potentiating tangle formation reduces acute toxicity of soluble tau species in the rat. *Brain* **141**: 535-549.

766

767

768

769 **Abbreviations-** Alzheimer disease (AD), brain-derived enriched extracellular vesicles (BD-EVs), brain-derived
770 fluid (BD-fluid), extracellular vesicles (EVs), Fluorescence Resonance Energy Transfer (FRET), Gene
771 Ontology Cellular Components (GOCC), immunohistochemistry (IHC), Intensity-based absolute quantification
772 (IBAQ), interstitial fluid (ISF), Monoclonal antibody (mAb), nanoparticle tracking analysis (NTA), neurofibrillary
773 tangles (NFT), Pick's disease (PiD), paraformaldehyde (PFA), phosphate buffered saline (PBS),
774 phenylmethylsulphonyl fluoride (PMSF), progressive supranuclear palsy (PSP), proteinase K (PK), repeat domain
775 (RD), room temperature (RT), size-exclusion chromatography (SEC).

776

777 **Figure legends-**

778

779 **Figure 1- Murine BD-EVs characterization-** Vesicles from murine BD-fluid were isolated using SEC to separate
780 vesicles from free-floating proteins. They were separated by sepharose resin columns in PBS and 500 μ l per
781 fraction were collected. (A) BD-EVs concentration was quantified per fraction using NTA and expressed as
782 vesicles/ml (A, black columns); the amount of total protein was determined using either UV spectrophotometry
783 (A, white columns) or a silver gel coloration (B). (C) The vesicles' morphology was studied using electron
784 microscopy in pooled fractions 1-4 (F1-4). The scale bar is indicated on the figure. (D) The vesicles' size
785 distribution was determined using NTA in pooled fractions 1-4 (F1-4). (E) Circular barplot showing IBAQ
786 intensity scores obtained for 20 selected GOCC terms after quantitative proteomic analysis of F1-4 fractions. (F)
787 Table listing human gene names corresponding to proteins recommended by MISEV 2018 detected in the F1-4
788 fractions after MS-based proteomic analysis. * used for families of multiple proteins, for example for
789 integrins: ITGA* indicates any integrin alpha chain. (G) The intravesicular tau (+PK-RIPA, with RIPA for ELISA
790 tau detection) or the intra- plus the extravesicular tau (-PK+RIPA) was quantified using ELISA from murine BD-
791 EVs (3 months-old THY-tau30). A positive control showing the global lysis of tau was also shown (+PK+RIPA).
792 ns= not significant. For A and D, mean of 3 independent experiences are shown, for B and C, illustrative data are
793 representative of at least 3 independent experiences.

794

795 **Figure 2- BD-EVs of a transgenic mouse model of tauopathy contain tau seeds-** (A) BD-EVs of TgAPP/PS1
796 (6 months old, n = 6), wild-type littermate mice (1 [n = 8], 3 [n = 6], and 6 [n = 8] months old), and THY-tau30
797 (1 [n = 7], 3 [n = 8], and 6 [n = 8] months old) were applied to the HEK-tau biosensor cells, and the FRET signal
798 was quantified using flow cytometry. 2 μ M of sonicated K18 fibrils were used as a positive control (+) and PBS

799 was used as a negative control (-). (B) BD-EVs isolated from 3-month-old THY-tau30 (F1-4) were further
800 ultracentrifuged to deplete vesicles. Pellet containing vesicles (P) and supernatant (S) were applied to the biosensor
801 assay. (C) Tau ELISA after tau immunodepletion (with or without sonication) from BD-EVs isolated from 3-
802 month-old THY-tau30. HT7 was used to immunodeplete tau whereas IgG1 was used as a negative control of
803 immunodepletion. (D) After tau immunodepletion of sonicated BD-EVs, fractions were applied to the biosensor
804 assay. For A, B and D, results are expressed as the percentage of the FRET signal x MFI (% FRET x MFI). * p <
805 0.05; ** p < 0.01; # p < 0.05, ##### p < 0.0001, or **** p < 0.0001.

806

807 **Figure 3- Tau lesions in human brain tauopathies-** Prefrontal (PF), occipital (OC) and cerebellum (Cb) brain
808 regions were dissected post-mortem from non-demented controls (n = 5), patients with PSP (n = 5), PiD (n = 5),
809 and AD (n = 10). (A) IHC of tau lesions using the AT8 antibody in mirror zones. Scale bars are indicated on the
810 figure. (B) Human brain sections were blindly quantified using QuPath-0.2.1 software. Results are expressed as a
811 percentage of tau lesions ([AT8 positive pixels/total pixels] x100). * p < 0.05; ** p < 0.01; *** p < 0.001, or **** p <
812 0.0001.

813

814 **Figure 4- Seed-competent species are found in BD-EVs in human tauopathies-** BD-fluid was purified from
815 the different brain regions and vesicles were isolated from the 500 µl of BD-fluid. (A) BD-EVs concentration was
816 analyzed using NTA and expressed as vesicles per gram/ml of tissue used to prepare the BD-fluid, and (B) global
817 tau content was determined by ELISA (INNOTEST® hTAU Ag, Fujirebio). Results are expressed as Tau (pg/ml)
818 / g of tissue. (C) BD-EVs were applied to the HEK-tau biosensor cells and the FRET signal was quantified using
819 flow cytometry. Results are expressed as % FRET x MFI / g of tissue. (D) Non-parametric Spearman correlation
820 between the post-mortem delay (PMD) and the FRET signal generated by BD-EVs from the AD prefrontal cortex
821 (PF), AD occipital cortex (OC), and AD cerebellum (Cb) regions. * p < 0.05; *** p < 0.001.

822

823 **Figure 5- AD BD-EVs efficiently seed host human mutated tau in young THY-tau30 mice-** (A) Four AD, four
824 PiD, four PSP, and four non-demented control BD-fluid were purified (Table 1 in bold), and isolated vesicles were
825 pooled. 2 µl (6x10⁹ vesicles) were applied to the HEK-tau biosensor cells, and the FRET signal was quantified
826 using flow cytometry. Results are expressed as % FRET x MFI. (B) BD-EVs (6x10⁹) were bilaterally injected into
827 the hippocampi of 1-month-old THY-tau30 or wild-type mice littermates (n = 5). Mice were sacrificed four weeks
828 post-injection and the tau pathology was analysed by DAB-immunostaining with the MC1 (upper) or AT100

829 (lower) antibodies. Sections from the hippocampus (injection site) are shown. Scale bars are indicated on the
830 figure. (C) The number of MC1 (left) or AT100 (right) immunoreactive neurons per brain section was quantified
831 (Bregma -2.3 to -2.8 mm), and the data are presented as mean \pm SD. ** $p < 0.01$, *** $p < 0.001$.

832

833 **Supplementary Figure Legends**

834

835 **Figure S1- HSP90 and CD63 are found associated to F1-4-** (A) The presence of the HSP90 in murine BD-EVs
836 (F1-4) is validated by western-blot. (B) The presence of the CD63 in human BD-EVs (F1-4) is validated by
837 immunogold electron microscopy.

838

839 **Figure S2- Tau lesions in THY-tau30 mice-** Illustration of tau lesions in hippocampal sections of TgAPP/PS1
840 (6 months old), wild-type littermate mice, and THY-tau30 (1, 3, and 6 months old) using antibodies that recognize
841 pathological forms of tau, MC1 (a-g) or AT100 (h-n). In f-n, a few neurofibrillary tangles are shown (arrows).
842 Scale bars are indicated on the figure. Enlargements of CA1 layers (squares) are shown at 6 months for THY-
843 tau30 mice. Pyr= Pyramidal, DS= Dorsal Subiculum, LMol = Lacunosum Molecular layer.

844

845 **Figure S3- Human BD-EVs characterization-** BD-EVs were isolated from BD-fluid using SEC to separate
846 vesicles from free-floating proteins and 500 μ l per fraction were collected. (A) BD-EVs concentration was
847 quantified in a NTA and expressed as vesicles/ml (A, black columns); the amount of total protein was determined
848 using either UV spectrophotometry (A, white columns) or a silver gel coloration (B). (C) The BD-EVs morphology
849 was studied using electron microscopy for pooled fractions 1-4 (F1-4). The scale bars are indicated on the figure.
850 (D) The vesicles' size distribution was studied using NTA in pooled fractions 1-4 (F1-4). (E) Circular barplot
851 showing IBAQ intensity scores obtained for different 20 selected GOCC terms after quantitative proteomic
852 analysis of F1-4 fractions. (F) Table listing human gene names of proteins recommended by MISEV 2018 detected
853 in the F1-4 fractions after MS-based proteomic analysis. * used for families of multiple proteins, for example for
854 integrins: ITGA* indicates any integrin alpha chain. For A and D, mean of 3 independent experiences are shown;
855 for B and C, illustrative data are representative of at least 3 independent experiences.

856

857 **Figure S4- Tau transfer by EVs.** (A) The htau1N4R-V5 isoform was expressed in HeLa cells using lentiviral
858 technology. (B) EVs isolated from the media and applied to receiving cells that don't express htau1N4R-V5 were

859 found to transfer tau between cells. In (A) and (B) tau is visualized in red with a V5 antibody; the nuclei are
860 labelled with DAPI and visualized in blue. (C and D) Primary neurons were either infected or not infected with
861 lentiviral vectors to overexpress htau-1N4R-V5, and the EVs isolated from the supernatant were injected into the
862 hippocampi of naïve rats. Confocal micrographs show hippocampal neurons (NeuN+: green) positive for
863 htau1N4R-V5, 50 days after the intrahippocampal injections of both the control EVs (C) and the EVs derived from
864 the htau1N4R primary culture (D). Scale bars are indicated on the figure.

865

866 **Table 1- Demographic, biological, and clinical characteristics of the human brain sample donors-** Brain
867 samples used for BD-fluid isolation are listed (n = 5 non-demented controls, n = 10 AD, n = 10 PSP, and n = 5
868 PiD). The items in bold indicate the AD patients, PSP patients, PiD patients, and non-demented controls selected
869 for the intracranial delivery of the BD-EVs in mice.

870

| Sex | Death (y) | PMI (h) | Diagnosis | Tau lesions | Braak | Thal | Cause of death |
|-----|-----------|---------|-----------|-----------------|-------|------|------------------------|
| M | 78 | 19 | Control | none | 0 | 0 | invasive aspergillosis |
| F | 82 | NA | Control | none | I | 1 | pericarditis |
| M | 23 | 24 | Control | none | 0 | 0 | myocarditis |
| M | 59 | 13 | Control | none | 0 | 0 | Septic shock |
| M | 41 | 11 | CTRL | none | 0 | 0 | suffocation |
| M | 70 | 30 | AD | NFT | VI | 4 | |
| F | 63 | 15 | AD | NFT | VI | 4 | |
| F | 60 | 24 | AD | NFT | VI | 5 | |
| F | 82 | 84 | AD | NFT | VI | 5 | |
| F | 87 | 24 | AD | NFT | VI | 5 | |
| F | 71 | 4 | AD | NFT | VI | 4 | |
| M | 64 | 20 | AD | NFT | VI | 4 | |
| M | 66 | 27 | AD | NFT | VI | 5 | |
| F | 66 | 16 | AD | NFT | VI | 4 | |
| M | 69 | 6 | AD | NFT | VI | 4 | |
| M | 74 | 9 | PSP | NFT and GFT | NA | 1 | |
| M | 90 | 36 | PSP | NFT and GFT | NA | 2 | |
| M | 88 | 3 | PSP | NFT and GFT | NA | 4 | |
| M | 69 | 17 | PSP | NFT and GFT | NA | 0 | |
| F | 79 | 4 | PSP | NFT and GFT | NA | 0 | |
| M | 65 | 18 | PSP | NFT and GFT | NA | 0 | |
| M | 82 | 4 | PSP | NFT and GFT | NA | 0 | |
| M | 64 | 18 | PSP | NFT and GFT | NA | 0 | |
| F | 77 | 9 | PSP | NFT and GFT | NA | 3 | |
| M | 57 | 20 | PSP | NFT and GFT | NA | 1 | |
| M | 57 | 22 | PiD | Pick bodies | NA | 0 | |
| M | 71 | 21 | PiD | Pick bodies | NA | 3 | |
| F | 78 | 11 | PiD | Pick bodies&NFT | NA | 0 | |
| M | 68 | 15 | PiD | Pick bodies | NA | 0 | |
| M | 68 | 8 | PiD | Pick bodies | NA | 0 | |

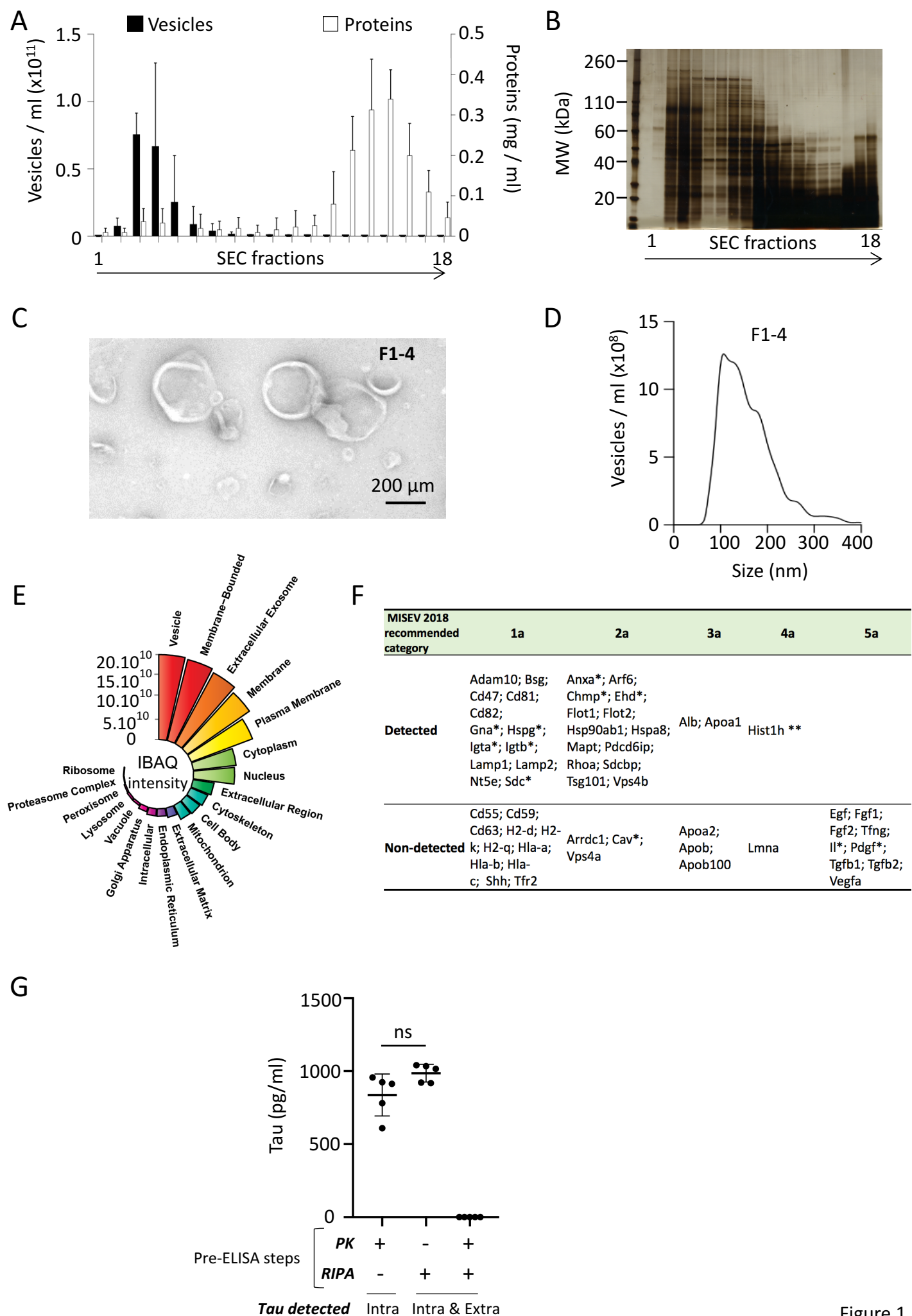


Figure 1

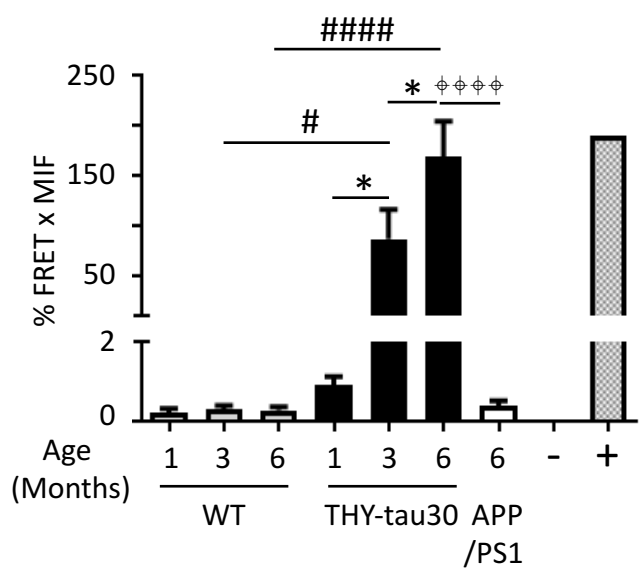
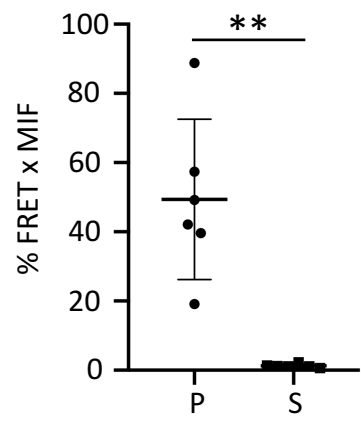
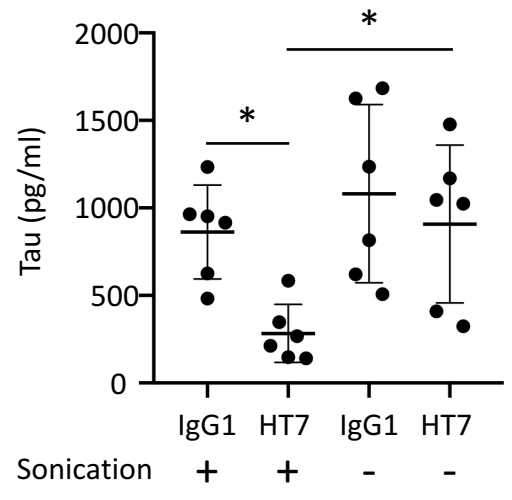
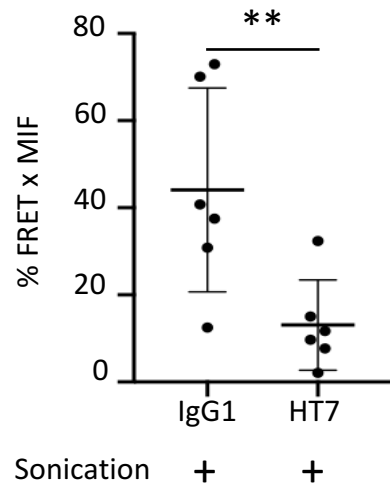
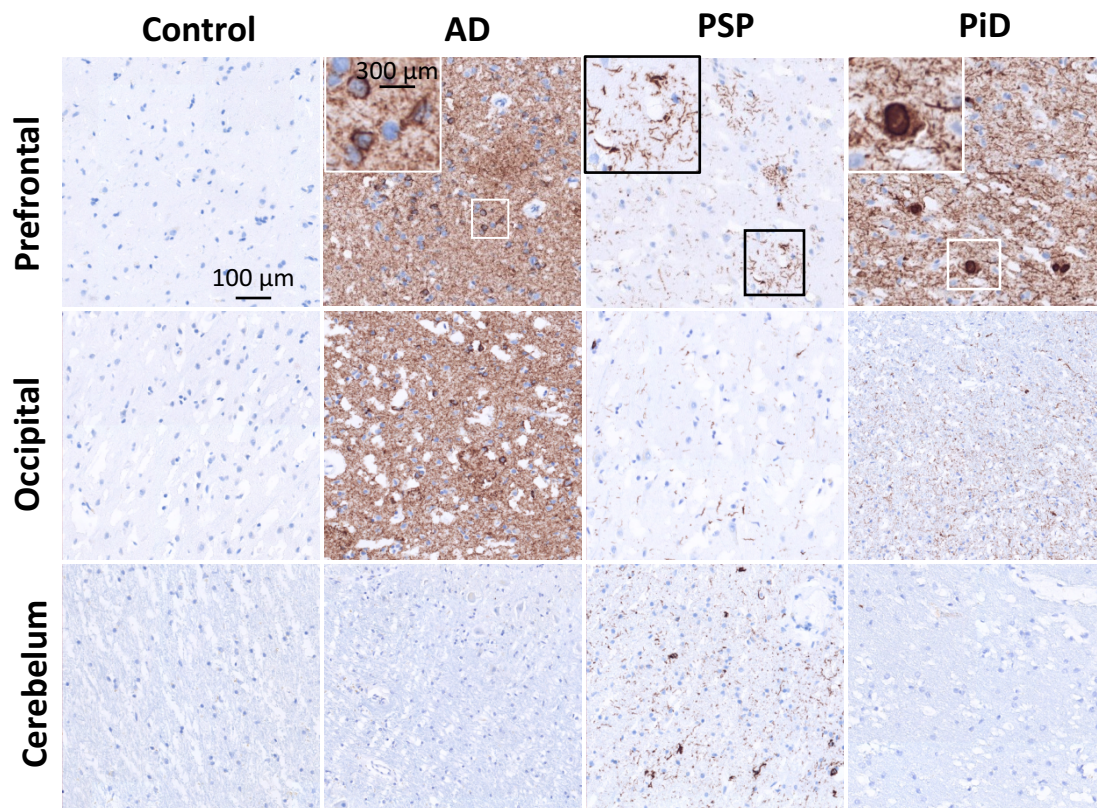
A**B****C****D**

Figure 2

A



B

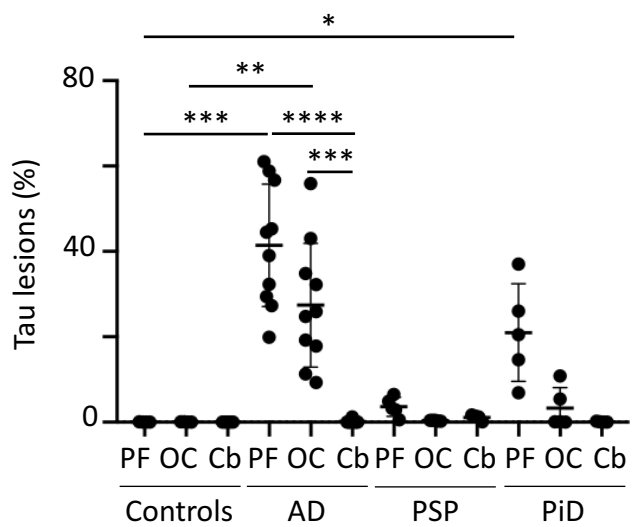
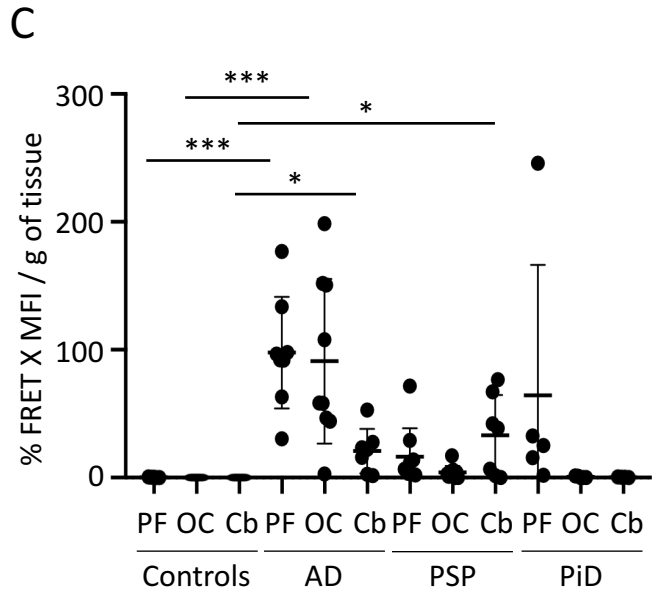
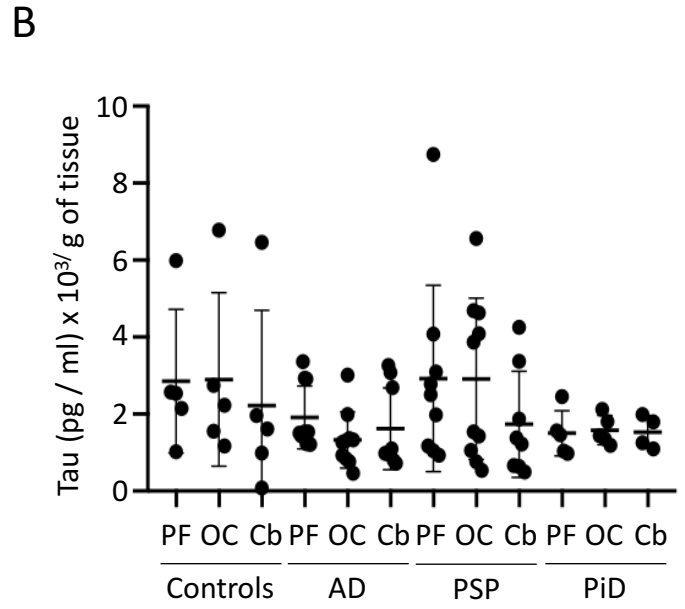
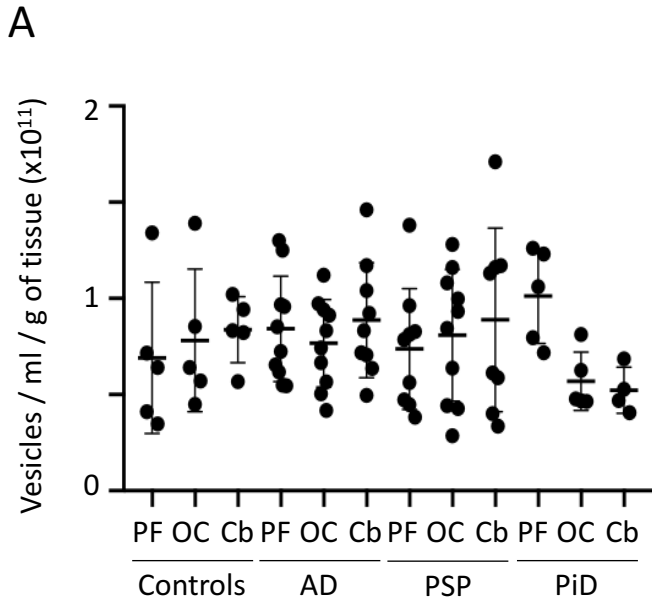


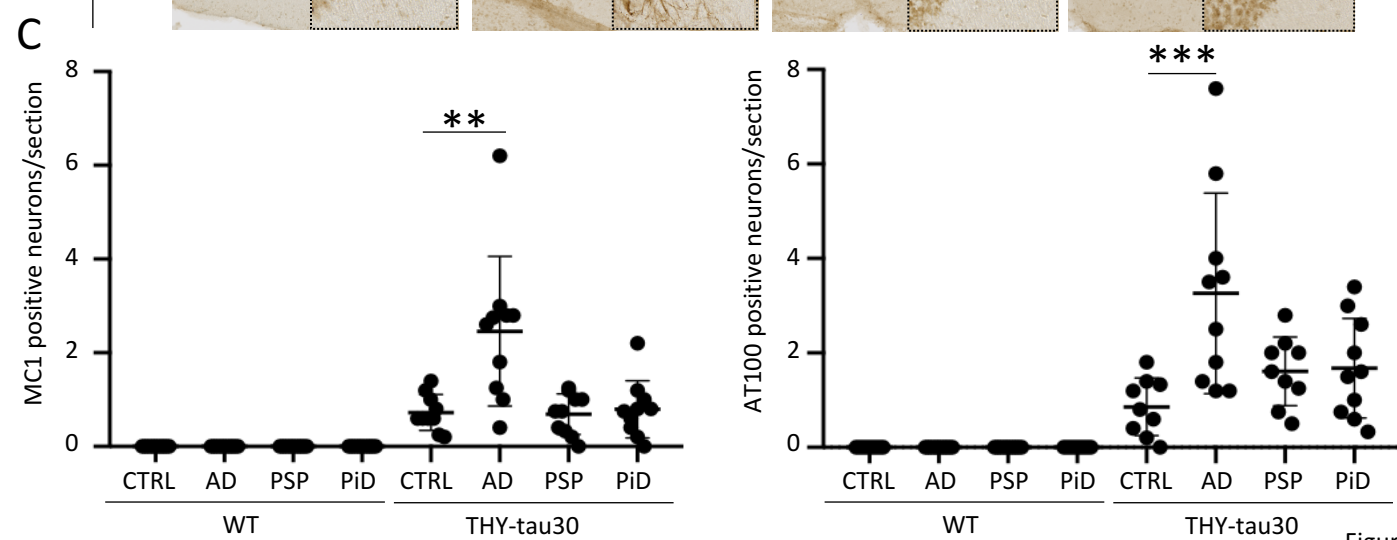
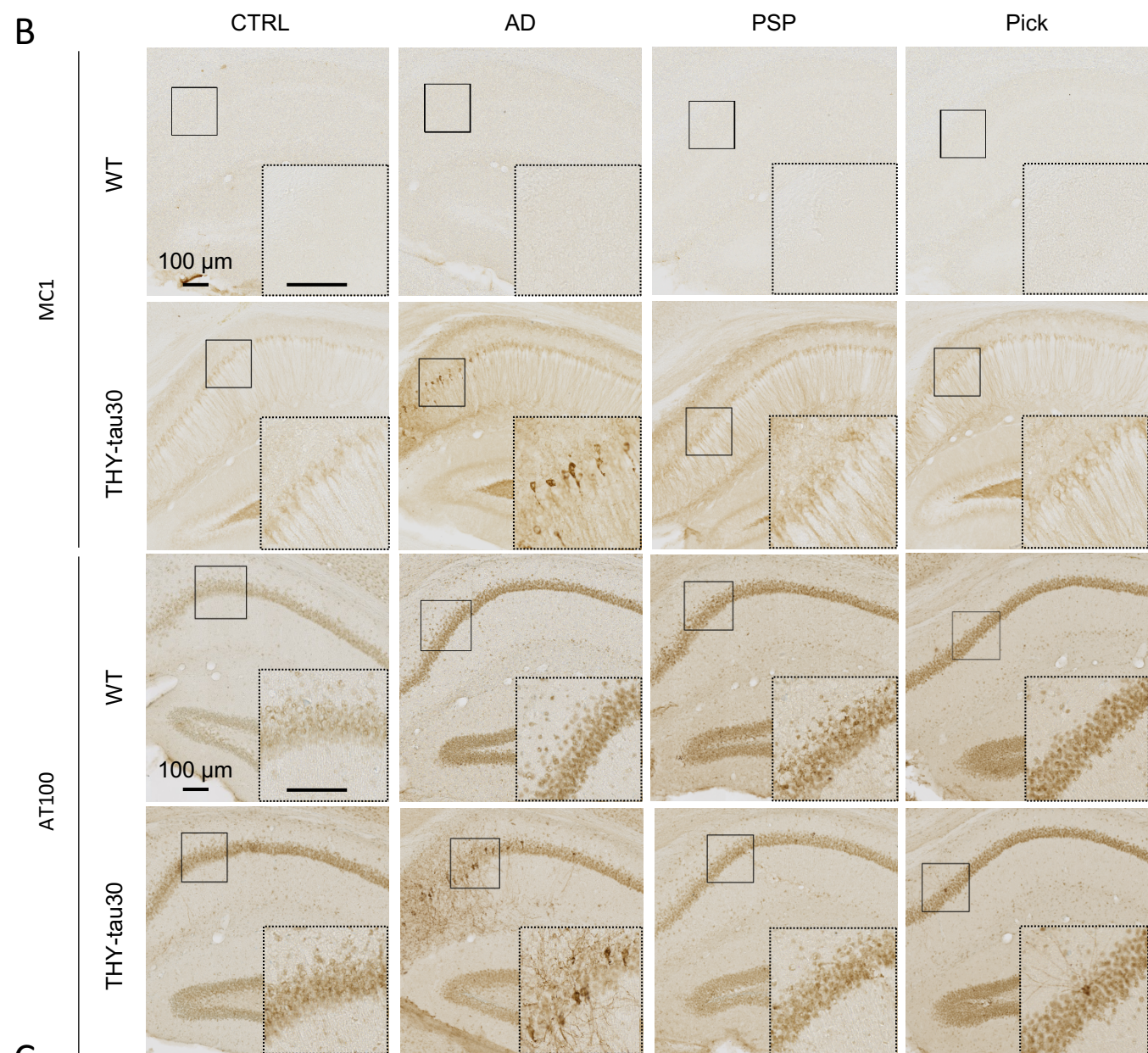
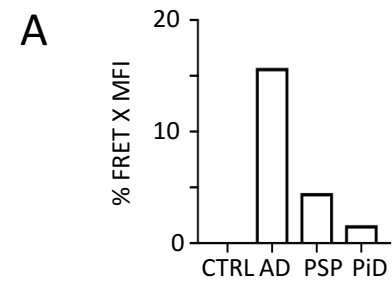
Figure 3



D

| PMD versus. | PF-AD | OC-AD | Cb AD |
|----------------------|---------|---------|--------|
| Spearman (r) | -0.6587 | -0.6307 | 0.1 |
| P value (two-tailed) | 0.0839 | 0.1413 | 0.9500 |
| P value summary | NS | NS | NS |

Figure 4



Supplementary information's

Extracellular vesicles: major actors of heterogeneity in tau spreading among human tauopathies

Elodie Leroux^{1†}, Romain Perbet^{1†}, Raphaëlle Caillerez¹, Kevin Richetin^{2,3,4}, Sarah Lieger¹, Jeanne Espourteille², Thomas Bouillet¹, Séverine Bégard¹, Clément Danis¹, Anne Loyens¹, Nicolas Toni², Nicole Déglon^{3,4}, Vincent Deramecourt¹, Susanna Schraen-Maschke¹, Luc Buée^{1*} and Morvane Colin^{1*}

Short title: EVs in pathological tau propagation

Supplementary Figure Legends

Figure S1- HSP90 and CD63 are found associated to F1-4- (A) The presence of the HSP90 in murine BD-EVs (F1-4) is validated by western-blot. (B) The presence of the CD63 in human BD-EVs (F1-4) is validated by immunogold electron microscopy.

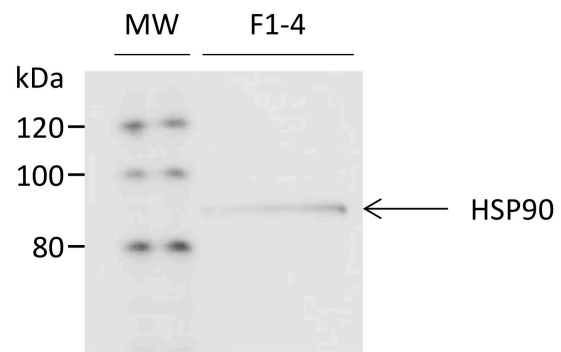
Figure S2- Tau lesions in THY-tau30 mice- Illustration of tau lesions in hippocampal sections of TgAPP/PS1 (6 months old), wild-type littermate mice, and THY-tau30 (1, 3, and 6 months old) using antibodies that recognize pathological forms of tau, MC1 (a-g) or AT100 (h-n). In f-n, a few neurofibrillary tangles are shown (arrows). Scale bars are indicated on the figure. Enlargements of CA1 layers (squares) are shown at 6 months for THY-tau30 mice. Pyr= Pyramidal, DS= Dorsal Subiculum, LMol = Lacunosum Molecular layer.

Figure S3- Human BD-EVs characterization- BD-EVs were isolated from BD-fluid using SEC to separate vesicles from free-floating proteins and 500 µl per fraction were collected. (A) BD-EVs concentration was quantified in a NTA and expressed as vesicles/ml (A, black columns); the amount of total protein was determined using either UV spectrophotometry (A, white columns) or a silver gel coloration (B). (C) The BD-EVs morphology was studied using electron microscopy for pooled fractions 1-4 (F1-4). The scale bars are indicated on the figure. (D) The vesicles' size distribution was studied using NTA in pooled fractions 1-4 (F1-4). (E) Circular barplot showing IBAQ intensity scores obtained for different 20 selected GOCC terms after quantitative proteomic analysis of F1-4 fractions. (F) Table listing human gene names of proteins recommended by MISEV 2018 detected in the F1-4 fractions after MS-based proteomic analysis. * used for families of multiple proteins, for example for

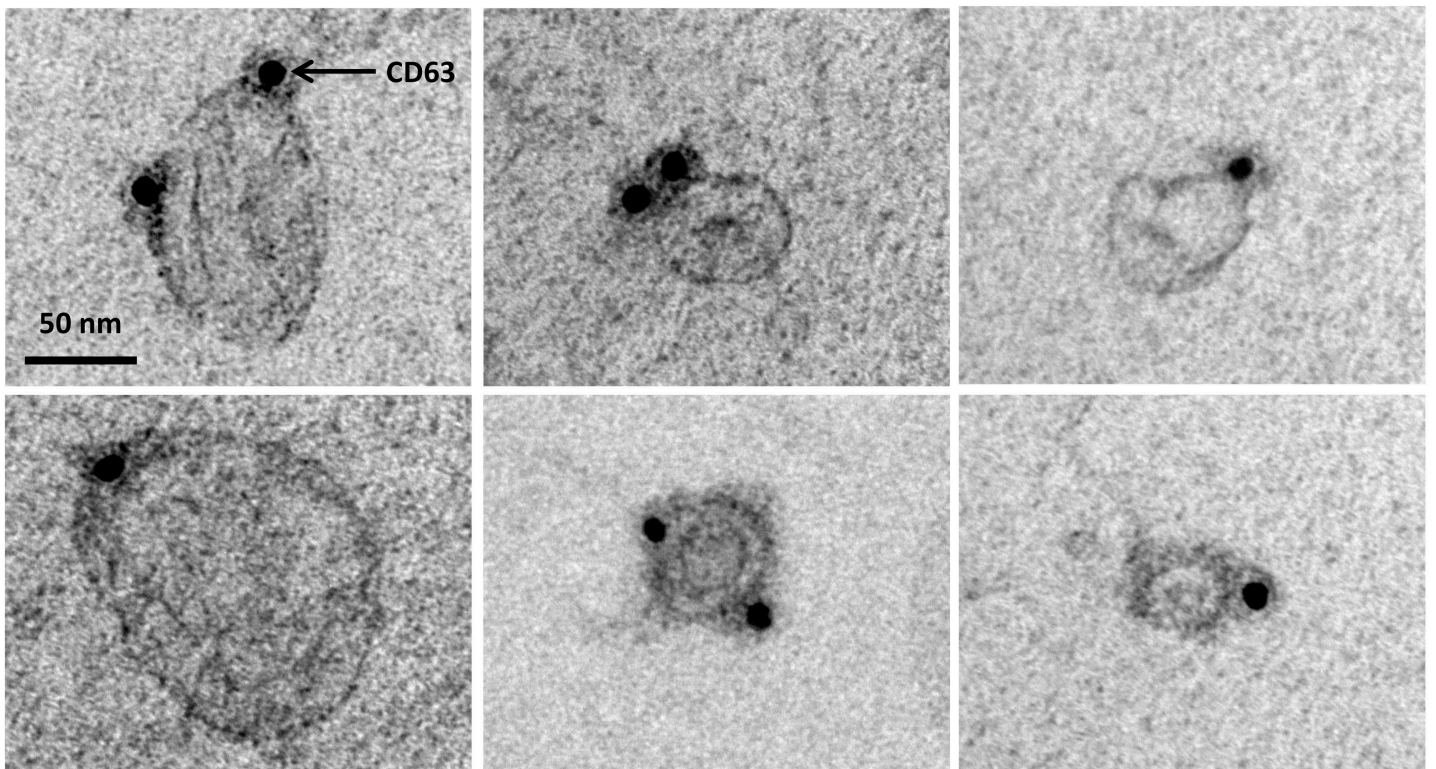
integrins: ITGA* indicates any integrin alpha chain. For A and D, mean of 3 independent experiences are shown; for B and C, illustrative data are representative of at least 3 independent experiences.

Figure S4- Tau transfer by EVs. (A) The htau1N4R-V5 isoform was expressed in HeLa cells using lentiviral technology. (B) EVs isolated from the media and applied to receiving cells that don't express htau1N4R-V5 were found to transfer tau between cells. In (A) and (B) tau is visualized in red with a V5 antibody; the nuclei are labelled with DAPI and visualized in blue. (C and D) Primary neurons were either infected or not infected with lentiviral vectors to overexpress htau-1N4R-V5, and the EVs isolated from the supernatant were injected into the hippocampi of naïve rats. Confocal micrographs show hippocampal neurons (NeuN+: green) positive for htau1N4R-V5, 50 days after the intrahippocampal injections of both the control EVs (C) and the EVs derived from the htau1N4R primary culture (D). Scale bars are indicated on the figure

A



B



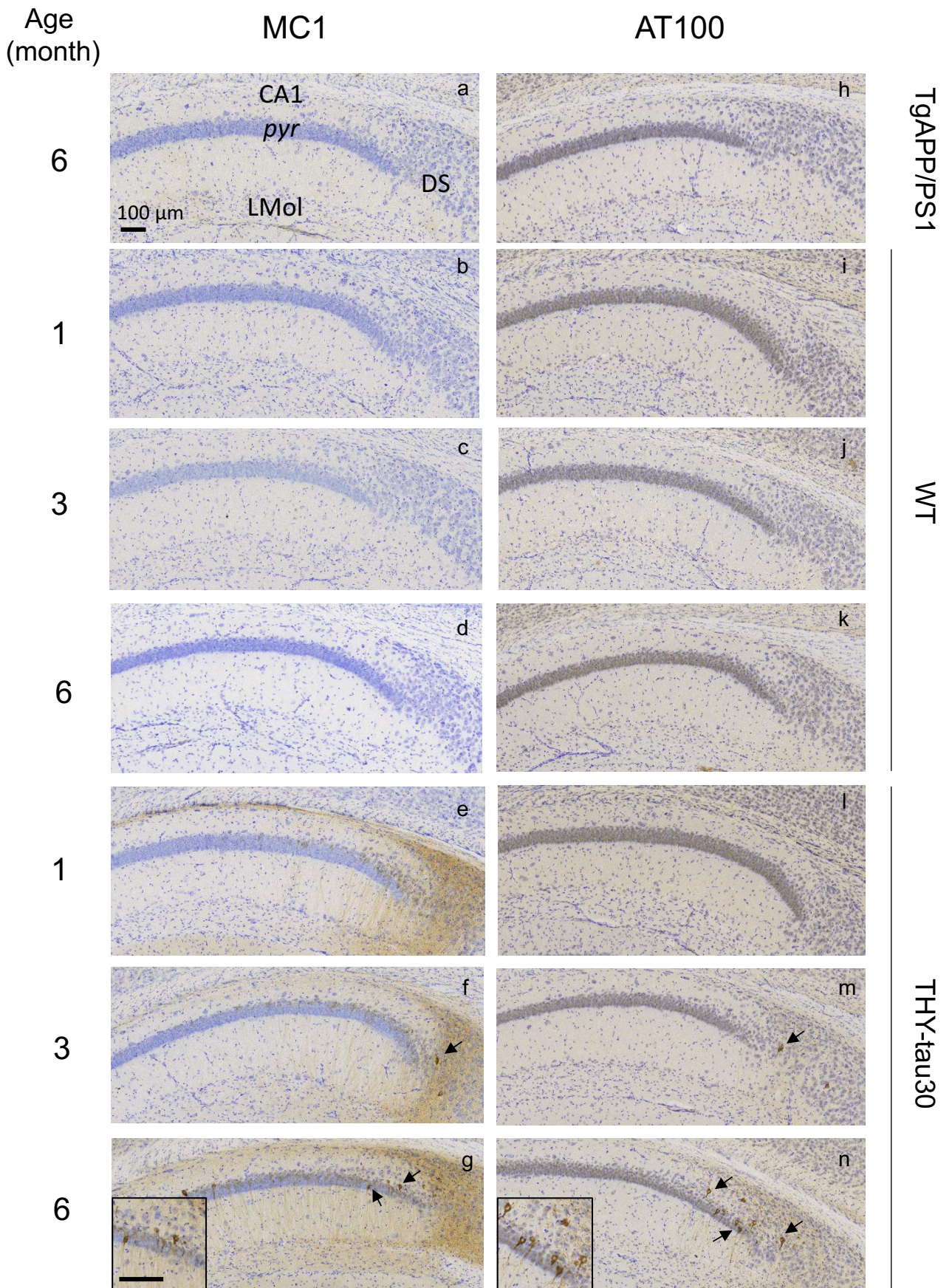
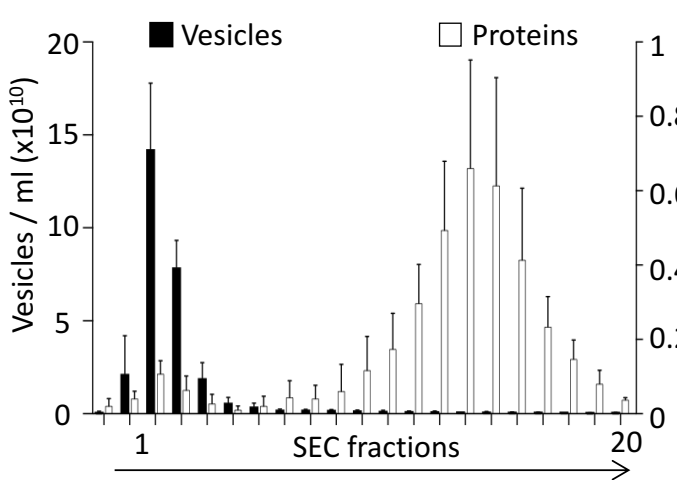
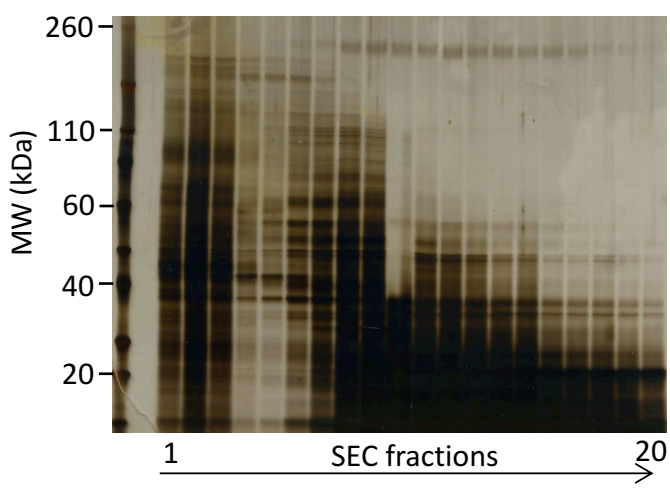


Figure Supp 2

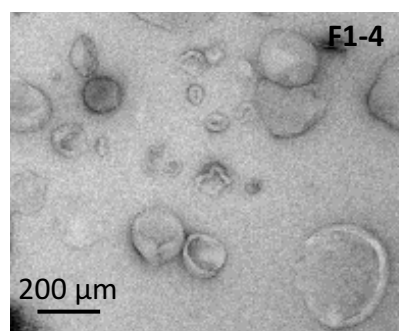
A



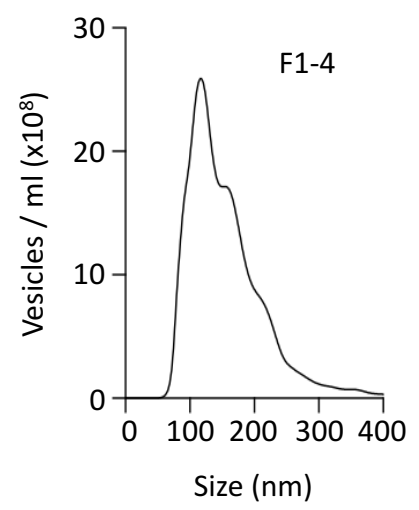
B



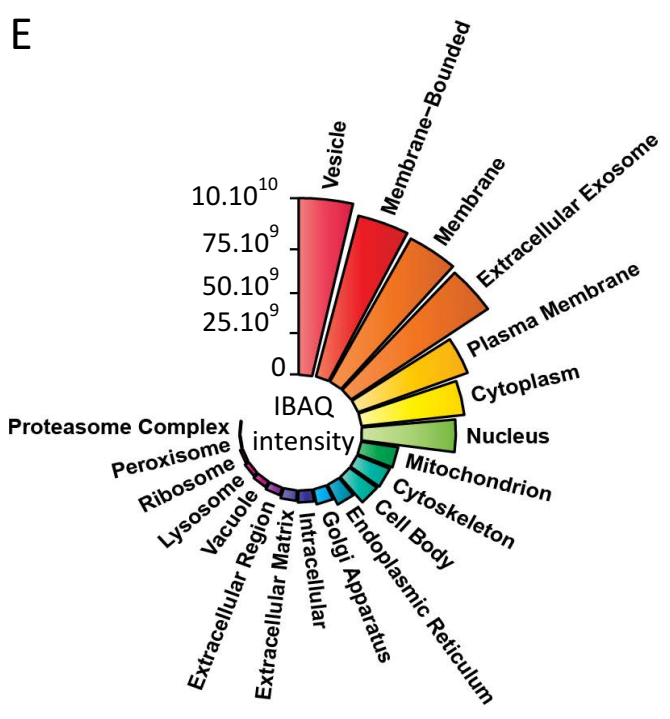
C



D



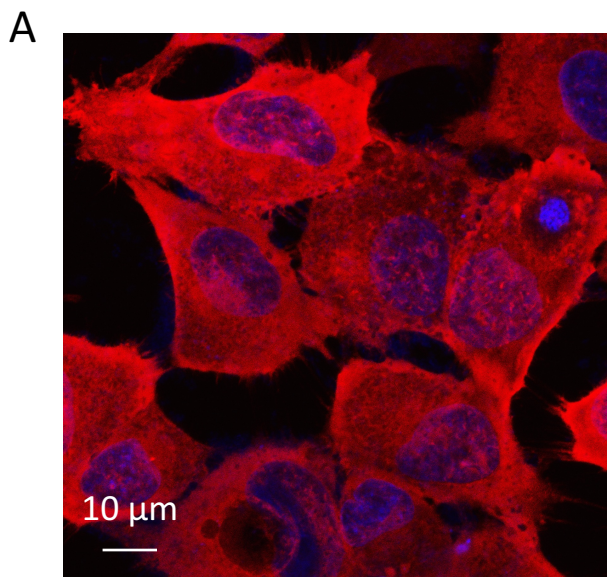
E



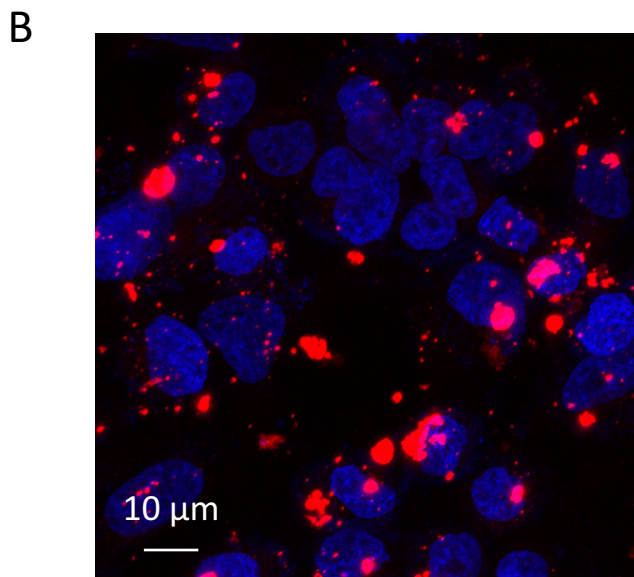
F

| MISEV 2018 recommended category | 1a | 2a | 3a | 4a | 5a |
|---------------------------------|---|--|---------------------|------------------|--|
| Detected | ADAM10; BSG; CD47; CD55; CD59; CD63; CD81; CD82; GNA*; HLA-A; HSPG*; IGTA*; IGTB*; LAMP1; LAMP2; NT5E; SDC* | ANXA*; ARF6; CAV*; CHMP*; EHD*; FLOT1; FLOT2; HSP90AB1; HSPA8; MAPT; PDGCR6IP; RHOA; SDCBP; TSG101; VPS4A; VPS4B | APOA1; APOB; | HIST1H*; LMNA | FGF1 |
| Non-detected | H2-D; H2-K; H2-Q; HLA-B; HLA-C; SHH; TFR2 | ARRDC1 | APOA2; APOB100; ALB | | EGF; FGF2; TFNG; IL*; PDGF*; TGFB1; TGFB2; VEGFA |

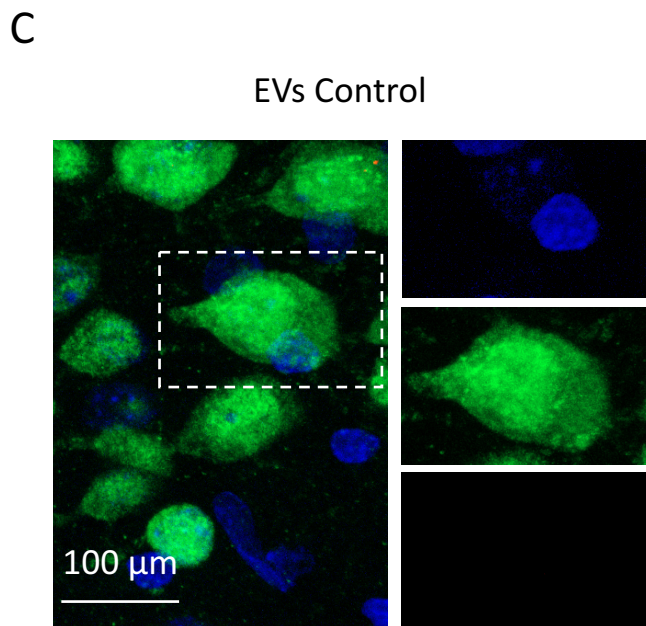
Figure Supp 3



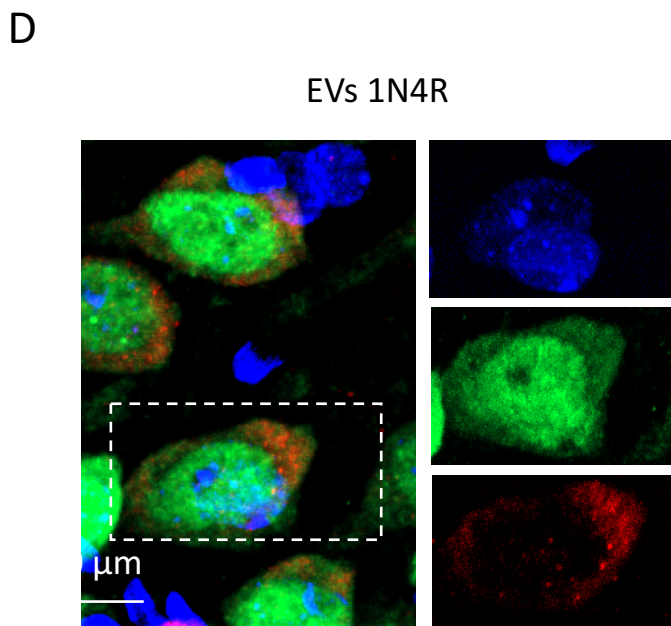
TauV5, donor cells



TauV5, receiving cells



DAPI / NeuN / V5



DAPI / NeuN / V5